MONOGRAPH

No. 39

2012

Kari Kallio

Water quality estimation by optical remote sensing in boreal lakes

MONOGRAPHS of the Boreal Environment Research

MONOGRAPHS OF THE BOREAL ENVIRONMENT RESEARCH

39

Kari Kallio

Water quality estimation by optical remote sensing in boreal lakes

Yhteenveto: Vedenlaadun arviointi kaukokartoituksen avulla boreaalisissa järvissä

The publication is available in the internet:
www.environment.fi/publications

ISBN 978-952-11-3947-5 (pbk.)
ISBN 978-952-11-3948-2(PDF)
ISSN 1239-1875 (print.)
ISSN 1796-1661 (online)

Edita Prima Ltd
Helsinki 2012

Contents

List of original publications and author's contributions

This thesis is a synthesis of the following publications referred in the text by PI–PVI. In addition, some previously unpublished results are presented.

PI Kallio, K., Pulliainen, J. & Ylöstalo, P. 2005. MERIS, MODIS and ETM channel configurations in the estimation of lake water quality from subsurface reflectance with semi-analytical and empirical algorithms. Geophysica 41: 31–55.

PII Kallio, K. 2006. Optical properties of Finnish lakes estimated with simple bio-optical models and water quality monitoring data. Nordic Hydrology 37: 183–204.

PIII Kallio K., Kutser, T., Hannonen T, Koponen S, Pulliainen J. Vepsäläinen J. & Pyhälahti T. 2001. Retrieval of water quality variables from airborne spectrometry of various lake types in different seasons. The Science of The Total Environment 268: 59–77.

PIV Kallio K., Koponen S. & Pulliainen J. 2003. Feasibility of airborne imaging spectrometry for lake monitoring - a case study of spatial chlorophyll a distribution in two meso-eutrophic lakes. International Journal of Remote Sensing 24: 3771–3790.

PV Kutser T., Pierson, D., Tranvik, L., Reinart, A., Sobek, S. & Kallio K. 2005. Estimating the colored dissolved organic matter absorption coefficient in lakes using satellite remote sensing. Ecosystems 8: 709–720.

PVI Kallio, K., Attila, J., Härmä, P., Koponen, S., Pulliainen, J., Hyytiäinen, U.-M. & Pyhälahti, T. 2008. Landsat ETM+ Images in the Estimation of Seasonal Lake Water Quality in Boreal River Basins. Environmental Management 42: 511–522.

	PI	**PII**	**PIII**	**PIV**	**PV**	**PVI**
Original idea	KK	KK	KK	KK	DP, TK	KK
Study design	KK, PY, JP	KK	KK, TH, JP	KK, SK, JP	TK, KK, DP	KK, PH, UMH, TP
Data gathering	KK, PY	KK	KK, TH, JP, TH, TP	DP, AR	UMH, KK	
Data analyses	KK, JP, PY	KK	KK, TK, TH, JP, JV	KK, SK, JP	TK, DP, AR, SS	KK, PH, JA, SK
Responsible for manuscript preparation	KK, JP	KK	KK	KK, JP	DP, TK, LT	KK
J. Attila (JA), T. Hannonen (TH), U.-M. Hyytiäinen (UMH), P. Härmä (PH), K. Kallio (KK), S. Koponen (SK) , T. Kutser (TK), D. Pierson (DP), J. Pulliainen (JP), T. Pyhälahti (TP), A. Reinart (AR), S. Sobek (SS), L. Tranvik (LT), J. Vepsäläinen (JV), P. Ylöstalo (PY)						

List of acronyms

AISA	Airborne Imaging Spectrometer for Applications
ALI	Advanced Land Imager
AOD	Aerosol Optical Depth
CDOM	Coloured Dissolved Organic Matter
CHRIS	Compact High Resolution Imaging Spectrometer
CPS	Colour Producing Substance
CZCS	Coastal Zone Colour Scanner
DN	Digital Number
EN	European Norm
EO-1	Earth Observation
ERTS 1	Earth Resources Technology Satellite
ESA	European Space Agency
ETM+	Enhanced Thematic Mapper Plus
FNU	Formazin Nephelometric Units
HIRLAM	High Resolution Limited Area Model
ICOL	Improved Contrast between Ocean and Land
IOP	Inherent Optical Properties
IR	Infrared
LDCM	Landsat Data Continuity Mission
LISS	Linear Imaging Self-Scanning System
MERIS	MEdium Resolution Imaging Spectrometer
MODIS	MODerate Resolution Imaging Spectroradiometer
MODTRAN	MODerate resolution atmospheric TRANsmission
MSI	Multi-Spectral Instrument
MSS	Mineral Suspended Solids
NASA	National Aeronautics and Space Administration
NIR	Near Infrared
OLCI	Ocean and Land Color Instrument
OLI	Operational Land Imager
PAR	Photosynthetically Active Radiation
PROBA	Project for On Board Autonomy
RMSE	Root Mean Squared Error
RRMSE	Relative Root Mean Squared Error
SeaWiFS	Sea-viewing Wide Field-of-view Sensor
SIOP	Specific Inherent Optical Property
SMAC	Simplified Method for the Atmospheric Correction
SNR	Signal-to-Noise Ratio
SPOT	Système Probatoire d'Observation de la Terre
TM	Thematic Mapper
TOA	Top Of Atmosphere
TSS	Total Suspended Solids
WFD	Water Framework Directive

List of symbols

$a_{cdom}(\lambda)$	Absorption coefficient of CDOM (m^{-1})
$a_{cdom}(400)$	Absorption coefficient of CDOM at 400 nm (m^{-1})
$a_{ph}(\lambda)$	Absorption coefficient of phytoplankton (m^{-1})
$a^*_{ph}(\lambda)$	Chl-a specific absorption coefficient of phytoplankton (m^2 mg^{-1})
$a_{tot}(\lambda)$	Total absorption coefficient (m^{-1})
$a_{tri}(\lambda)$	Absorption coefficient of tripton (m^{-1})
$a^*_{\underline{TSS}}$	Specific absorption coefficient of bleached total suspended solids (m^2 g^{-1})
$a^*_{\underline{TSS}}(400)$	Specific absorption coefficient of bleached total suspended solids at 400 nm (m^2 g^{-1})
$a_w(\lambda)$	Absorption coefficient of pure water (m^{-1})
b_{MSS}	Scattering coefficient of mineral suspended solids (m^{-1})
$b_{b,\,tot}(\lambda)$	Total backscattering coefficient (m^{-1})
$b_{b,\,ph}(\lambda)$	Backscattering coefficient of phytoplankton (m^{-1})
$\hat{b}_{bw}$	Backscattering ratio of pure water
$\hat{b}_{b,TSS}$	Backscattering ratio of TSS
b_{ph}	Scattering coefficient of phytoplankton (m^{-1})
$b_{tot}(\lambda)$	Total scattering coefficient (m^{-1})
$b^*_{TSS}(\lambda)$	Specific scattering coefficient of TSS (m^2 g^{-1})
$b^*_{TSS}(555)$	Specific scattering coefficient of TSS at 555 nm (m^2 g^{-1})
$b_w(\lambda)$	Scattering coefficient of pure water (m^{-1})
$c_{tot}(\lambda)$	Total beam attenuation coefficient (m^{-1})
C	Coefficient comprising the illumination dependencies
C_1, C_2	Empirical coefficients
$C_{Chl\text{-}a}$	Concentration of the sum of chlorophyll a and phaeophytin a (µg l^{-1})
Chl-a	sum of chlorophyll a and phaeophytin a
$\langle C_{Chl-a,ref} \rangle$	Mean $C_{Chl\text{-}a}$ of the discrete sampling stations (µg l^{-1})
$\langle C_{Chl-a,AISA} \rangle$	Mean AISA based estimate of $C_{Chl\text{-}a}$ (µg l^{-1})
C_{TSS}	Concentration of total suspended solids (mg l^{-1})
D_1, D_2	Empirical coefficients
$E_{\langle C_{Chl-a} \rangle}$	Observed error for the discrete $C_{Chl\text{-}a}$ data
E_u	Upwelling plane irradiance (W m^{-2} s^{-1})
E_d	Downwelling plane irradiance (W m^{-2} s^{-1})
g_1, g_2	Coefficients depending on the shape of the scattering phase function
K_d	Diffuse attenuation coefficient (m^{-1})
L_a	Radiance due to aerosol scattering (W m^{-2} s^{-1} sr^{-1})
L_{inst}	Radiance measured at instrument (W m^{-2} s^{-1} sr^{-1})
L_r	Radiance due to Rayleigh scattering by air molecules (W m^{-2} s^{-1} sr^{-1})

L_{sky}	Average radiance of that area of the sky that is specularly reflected into the sensor (W m^{-2} s^{-1} sr^{-1})
L_{surf}	Surface radiance (W m^{-2} s^{-1} sr^{-1})
L_w	Water leaving radiance (W m^{-2} s^{-1} sr^{-1})
M_S	Confidence interval
n	Number of samples in the training dataset
n_b	Scattering exponent
N	Number of data points
Q	Q-factor, ratio between upwelling irradiance and radiance (sr)
R^2	Coefficient of determination
R	Subsurface irradiance reflectance
R_{rs}	Remote sensing reflectance (sr^{-1})
s	Radiance reduction factor due to internal reflection and refraction
S	RMSE for algorithm training data
SE	Standard error
se	SE of the mean of the discrete observations
S_{CDOM}	Spectral slope coefficient of CDOM absorption (nm^{-1})
S_{tri}	Spectral slope coefficient of tripton absorption (nm^{-1})
$t_{\alpha/2}$	Coefficient based on the T_{n-2} distribution
T_{atm}	Atmospheric transmission factor
$Turb$	Turbidity (FNU)
$\langle X \rangle$	Mean of remotely sensed $C_{Chl\text{-}a}$ over the entire study area
$\langle X_{ref} \rangle$	Mean $C_{Chl\text{-}a}$ for the algorithm training data
z	Water depth (m)
z_{att}	Attenuation depth (m)
Z_{SD}	Secchi disk transparency (m)
β	Volume scattering function (sr^{-1} m^{-1})
$\tilde{\beta}$	Scattering phase function (sr^{-1})
θ_v	Zenith observation angle
θ_s	Solar zenith angle
σ_i	Standard deviation of statistical reflectance modelling error for channel i
σ_L	Fresnel reflectance
λ	Wavelength (nm)
λ_0	Cosine of the solar zenith angle in the water
ϕ_v	Azimuth observation angle
ψ	Scattering angle

Water quality estimation by optical remote sensing in boreal lakes

Kari Kallio

Department of Environmental Sciences, Faculty of Biological and Environmental Sciences, University of Helsinki

Kallio, K. 2012. Water quality estimation by optical remote sensing in boreal lakes. Monographs of the Boreal Environment Research No. 39. 54 p.

The monitoring of lakes is mainly based on collecting water samples, which are transported to a laboratory for analysis. In lake-rich regions, the gathering of information about water quality is challenging because only a small proportion of the lakes can be assessed each year. One of the techniques for improving the temporal and spatial representativeness of lake monitoring is remote sensing from aircrafts and satellites. The main objectives of this study were to investigate and test remote sensing interpretation algorithms for water quality estimation in Finnish lakes, to develop optical models for the needs of interpretation and for the estimation of light attenuation, and to study the advantages of using remote sensing data as compared to conventional monitoring methods. The experimental material included detailed optical measurements in 11 lakes, remote sensing measurements with concurrent *in situ* sampling, automatic raft measurements and a national dataset of routine water quality measurements. The analyses of the spatially high-resolution airborne remote sensing data from eutrophic and mesotrophic lakes showed that one or a few discrete water quality observations using conventional monitoring can yield a clear over- or underestimation of the overall water quality in a lake. The use of TM-type satellite instruments in addition to routine monitoring results substantially increases the number of lakes for which water quality information can be obtained. The preliminary results indicated that coloured dissolved organic matter (CDOM) can be estimated with TM-type satellite instruments, which could possibly be utilised as an aid in estimating the role of lakes in global carbon budgets. Based on the results of reflectance modelling and experimental data, MERIS satellite instrument has optimal or near-optimal channels for the estimation of turbidity, chlorophyll *a* and CDOM in Finnish lakes. MERIS images with a 300 m spatial resolution can provide water quality information in different parts of large and medium-sized lakes, and in filling in the gaps resulting from conventional monitoring. Algorithms that would not require simultaneous *in situ* data for algorithm training would increase the amount of remote sensing-based information available for lake monitoring. The MERIS Boreal Lakes processor, trained with the optical data and concentration ranges provided by this study, enabled turbidity estimations with good accuracy without the need for algorithm correction with *in situ* measurements, while chlorophyll *a* and CDOM estimations require further development of the processor. The accuracy of interpreting chlorophyll *a* via semi empirical algorithms can be improved by classifying lakes prior to interpretation according to their CDOM level and trophic status, and by creating lake-type-specific algorithms. The results of optical modelling showed that the spectral diffuse attenuation coefficient can be estimated with reasonable accuracy from the measured water quality concentrations. This provides more detailed information on light attenuation from routine monitoring measurements than is available through the Secchi disk transparency. This study improves the interpretation of water quality by remote sensing in boreal lakes and encourages the use of remote sensing in lake monitoring.

Keywords: lakes, remote sensing, MERIS, ETM+, optical modelling, light attenuation, turbidity, suspended solids, chlorophyll *a*, CDOM, monitoring

1 Introduction

1.1 Background

The aim of lake monitoring is to provide information on the status and temporal changes of lakes for the needs of reporting and decision-making. In an ideal case, monitoring information is three-dimensional, is temporally extensive and includes information for the estimation of relevant processes (Van Stokkom et al. 1993, Fisher 1994). Monitoring of lakes has long been based on collecting of water samples, which are transported to a laboratory for analysis. Currently, most of the lakes that are monitored are sampled at one point only, often in the deepest part of the lake. In lake-rich regions, only a small percentage of the lakes are monitored in the course of the year and usually are sampled only once in the ice-free season. The techniques proposed for improving the temporal and spatial representativeness of monitoring include automatic stations for continuous measurements (Tilak et al. 2007), transect measurements with optical instruments (e.g. Lindfors et al. 2005, Lepistö et al. 2010) and remote sensing via spectrometers installed aboard an aircraft or a satellite.

Remote sensing of water quality mainly employs passive instruments, which use the sun as their light source and measure the light reflected from a water body. Investigation of the use of satellite remote sensing for lake monitoring was under way already in the 1970s, after the launch of ERTS 1 (later named Landsat 1) in 1972 and a considerable amount of investigations has been published since then (see, for example, references in Bukata 2005). The early satellite instruments were designed for terrestrial applications. The first instrument designed specifically for the estimation of water quality (particularly chlorophyll *a*) was CZCS, aboard the Nimbus 7 satellite, which provided images in 1978–1986 with 825 m spatial resolution, followed by SeaStar SeaWiFS (1,000 m resolution, 1997–2011).

In the 2000s, the usability of satellite imagery for water quality mapping has improved considerably with the availability of several satellite instruments created for water applications in particular. Terra MODIS (2000–), Aqua MODIS (2002–) and ENVISAT MERIS (2002–) provide images daily and have several narrow channels optimised for water quality estimation. The low spatial resolution of these instruments (250 to 1,000 m), however, limits their use to only large and medium-sized lakes. In small lakes, satellite remote sensing is possible with Landsat-TM-type instruments (e.g. ETM+, SPOT, LISS and ALI), which typically have a 30-metre spatial resolution. Very high-resolution instruments, such as IKONOS, typically have a spatial resolution of 1–4 m and enable monitoring of aquatic macrophytes and water quality in ponds (Sawaya et al. 2003). The drawback of the TM-type and high-spatial-resolution instruments is that, since they were designed initially for terrestrial applications, their spectral resolution, measurement frequency and radiometric characteristics are not optimal for water quality mapping. Satellite instruments with good spectral and spatial resolution have hitherto been available only for research use (EO-1 Hyperion and CHRIS PROBA). Airborne remote sensing usually provides hyperspectral data with high spatial resolution from a limited area and has been used in algorithm development and in mapping of water quality in a single lake or a small group of lakes (e.g. Dekker 1993, Pulliainen et al. 2001).

At present, remote-sensing-based estimates of water quality are not routinely utilised in lake monitoring. Satellite images have been used in regional assessment of lake water quality (Kloiber et al. 2002a, Dekker et al. 2002, Koponen et al. 2004) , for the investigation of temporal trends (Kloiber et al. 2002b, Shuchman et al. 2006) and to track the evolution of algal bloom across a lake (e.g. Binding et al. 2011). In addition to shortcomings in the instrument configuration, hindrances to the wider use of remote sensing in lake monitoring include suspicions of the reliability of remote sensing (the accuracy of the estimates etc.), lack of programmes in place that would

provide ongoing products and the weather-dependency of remote sensing (cloud cover hampers the estimation of water quality) (Bukata et al. 2002).

The idea of remote sensing is to derive information on the optical properties and the concentrations of substances from variations in water colour. The low radiance levels of natural waters mean that remote sensing is more complicated for water than in the cases of many terrestrial objects. Consequently, remote sensing for water requires knowledge of aquatic optics and of the fate of light in the atmosphere. The theory of aquatic optics was mainly developed by Preisendorffer (1976) and the related radiance transfer equations were numeralised by Mobley (Mobley 1994, Mobley & Sundman 2007). Aquatic optics focused in its early years on ocean waters (e.g. Jerlov 1976, Morel & Prieur 1977) and optical measurements in lakes (Bukata et al. 1979, Kirk 1984, Dekker 1993) were rare. Lakes are usually optically more complex than are ocean waters and some of the optical methods developed for ocean waters had to be modified for lakes (e.g. Strömbeck 2001). In recent years, optical measurements for lakes have become more commonplace (e.g. Rijkeboer et al. 1998, Strömbeck 2001, Herlevi 2002, Arst 2003, Reinart et al. 2004, Dall'Olmo & Gitelson 2006b, Gallegos et al. 2008), partly because of the better availability of optical instruments. Besides remote sensing, knowledge of in-water optical properties and processes is needed in the estimation of light available for photosynthesis (Pierson et al. 2003), in ecosystem models (Luyten et al. 1999), in the modelling of photochemical mineralization of dissolved organic matter (Vähätalo et al. 2000), in the simulation of water temperature and in underwater visibility studies. Optical properties and models have also been utilised in selection of best practice in lake management (Effler et al. 2001, Jaun et al. 2007). In addition, direct measurement of optical properties (e.g. absorption and scattering coefficients) in field enables the estimation of water quality (e.g. Koponen et al. 2007).

Investigations of remote sensing of lake water quality have been carried out in several regions – e.g. those of large lakes and Lake Erken in Sweden (Lindel 1981, Strömbeck & Pierson 2001), Estonian lakes (Kutser 1997, Reinart et al. 2004), lakes in southern Finland (Herlevi 2002, Koponen et al. 2004), Russia's Lake Ladoga (Pozdnyakov 1998, Korosov et al. 2007), Lake Constance (Gege 1998, Heege & Fischer 2004) and other lakes in Germany (Thiemann & Kaufmann 2000), sub-alpine lakes (Brivio et al. 2001, Giardino et al. 2007) in Italy, eutrophic lakes in the Netherlands (Dekker 1993, Simis 2006), lakes and rivers in eastern Europe (Gitelson et al. 1993, Moses et al. 2009), the Great Laurentian lakes (Bukata et al. 1995, Binding et al. 2008), lakes in the USA's Wisconsin (Kloiber et al. 2002a) and China's Lake Taihu (Zhang et al. 2010). Most of the published investigations have included development and testing of interpretation algorithms as well as measurement of optical properties of water, which were utilised in algorithm development and validation. Recently, the Inland and Near-Coastal Water Quality Remote Sensing Working Group, in work initiated by the Group on Earth Observations, was created for promoting the use of remote sensing globally (GEO 2007, GEO 2011).

The water quality variables reported as able to be estimated by remote sensing in lakes are concentration of total suspended solids, turbidity, concentration of humic substances, concentration of chlorophyll *a*, occurrence of surface accumulating algal blooms, concentration of phycocyanin and Secchi disk transparency (e.g. Dekker 1993, Bukata et al. 1995, Pozdnyakov & Grassl 2003). One central aim in remote sensing of water quality is the development of algorithms, which would not require *in situ* sampling for algorithm training. This requires proper atmospheric correction, but standard atmospheric corrections are usually not directly valid/suitable for lakes (e.g. Simis 2006, Giardino et al. 2007, Moses et al. 2009). Atmospheric correction has turned out to be demanding particularly for oligotrophic lakes (Odermatt et al. 2010, Guanter et al. 2010).

The planned satellite missions will provide better remote sensing data for lake mapping than are currently available. For example, ESA's Sentinel-2 MSI (scheduled to be launched in 2012, with spatial resolution of 10–20 m) will make possible more accurate water quality estimates through enhanced channel configuration and better temporal resolution than the current TM-type

instruments allow. Better data for the needs of atmospheric correction will also be available, since MSI and Sentinel-3 OLCI, the follow-up of MERIS and scheduled for a 2013 launch, will have additional channels optimised for correcting atmospheric disturbances. New hyperspectral satellite instruments, such as EnMap (http://www.enmap.org/) and HyspIRI (http://hyspiri.jpl.nasa.gov/), are also in the planning or construction stage.

1.2 Basics of water optics and remote sensing

1.2.1 Colour-producing substances and their optical properties

Water colour is due to colour-producing substances (CPSs), which absorb or scatter light (the visible region of the electromagnetic radiation, VIS). Absorption and scattering coefficients (m^{-1}) are independent of the ambient light field and are therefore called inherent optical properties (IOPs, Preisendorfer 1976). Specific inherent optical property (SIOP) is IOPs expressed per unit mass of material. Apparent optical properties (AOPs) depend on the IOPs and on the directionality of the ambient light field (Preisendorfer 1976). Examples of AOPs are: remote sensing reflectance, diffuse attenuation coefficient and Secchi disk transparency.

The two fundamental IOPs are the absorption coefficient and the volume scattering function. Water typically includes three main groups of absorbing CPSs: phytoplankton, tripton (non-algal particles such as detritus and mineral particles) and coloured dissolved organic matter (CDOM). In addition, pure water absorbs light. The total spectral absorption coefficient ($a_{tot}(\lambda)$) can be described by

$$a_{tot}(\lambda) = a_w(\lambda) + a_{CDOM}(\lambda) + a_{ph}(\lambda) + a_{tri}(\lambda) \quad (1)$$

where $a_w(\lambda)$ is the absorption coefficient of pure water, $a_{ph}(\lambda)$ is the absorption coefficient of phytoplankton, $a_{CDOM}(\lambda)$ is the absorption coefficient of CDOM, $a_{tri}(\lambda)$ is the absorption coefficient of tripton and λ is wavelength.

The volume scattering function (β) describes how a volume of water is scattering light. The total scattering coefficient, $b_{tot}(\lambda)$, is obtained by integrating β over all scattering angles (ψ):

$$b_{tot}(\lambda) = 2\pi \int_0^{\pi} \beta(\psi, \lambda) \sin\psi \, d\psi \quad (2)$$

The angular pattern of the scattered light is given by the scattering phase function:

$$\tilde{\beta}(\psi, \lambda) = \frac{\beta(\psi, \lambda)}{b_{tot}(\lambda)} \quad (3)$$

$b_{tot}(\lambda)$ can be divided into the following main components contributing to scattering:

$$b_{tot}(\lambda) = b_w(\lambda) + b_{MSS}(\lambda) + b_{ph}(\lambda) \quad (4)$$

where b_w is the scattering coefficient of pure water, b_{MSS} is the specific scattering coefficient of mineral suspended solids and b_{ph} is the scattering coefficient of phytoplankton.

The corresponding equation for the backscattering component ($\pi/2 < \psi \leq \pi$) of b_{tot} is

$$b_{b,tot}(\lambda) = b_{b,w}(\lambda) + b_{b,MSS}(\lambda) + b_{b,ph}(\lambda) \quad (5)$$

The total attenuation coefficient, $c_{tot}(\lambda)$, is the sum of the absorption and scattering coefficients:

$$c_{tot}(\lambda) = a_{Tot}(\lambda) + b_{Tot}(\lambda) \quad (6)$$

Knowledge of the spectral absorption and scattering coefficients of CPSs is needed in, for example, bio-optical models, which can be formulated for total absorption, reflectance, diffuse attenuation coefficient etc. Next, the absorption and scattering properties and the inelastic processes of the main CPSs are briefly described.

Attenuation of light in pure water is dominated by absorption at wavelengths greater than 580 nm and by scattering in the blue region of the spectrum. Absorption and scattering coefficients of pure water have been reported by several researchers; see, for example, the Ocean optics protocols of NASA (2003). Absorption by pure water is weakly temperature-dependent, mainly in the near-infrared (NIR) region of the spectrum (Pegau et al. 1997).

In remote sensing and water optics, humic substances are commonly called coloured dissolved organic matter (CDOM), referring to the absorbing component of dissolved organic matter. Absorption by CDOM increases strongly with decreasing wavelength and is usually described by an exponential equation (Bricaud et al. 1981). Other proposed descriptions of $a_{CDOM}(\lambda)$ include Gaussian (Gege 2000) and hyperbolic (Twardowski et al. 2004) models. The absorption coefficient of CDOM at a fixed wavelength in the blue region (usually 400 or 440 nm) of the spectrum is used as an indirect measure of CDOM concentration. The spectral slope coefficient (S_{CDOM}) of the exponential equation depends on the type of CDOM; fulvic acids have been found to have higher S_{CDOM} than have humic acids (Carder et al. 1989, Hansel & Carlsson 2002). Based on these findings, two-component exponential models with different slopes of fulvic and humic acids have been proposed (Carder et al. 1989, Laanen 2007) instead of the single exponential function. Another factor influencing S_{CDOM} is photobleaching of CDOM, which increases S_{CDOM} (e.g. Twardowski & Donaghay 2002). The variations in the published S_{CDOM} can also be due to methodological reasons, such as differences in the spectral range used for S_{CDOM} estimation (Twardowski et al. 2004).

$a_{CDOM}(\lambda)$ is usually measured from filtered – preferably via a membrane filter with a 0.2 µm pore size (NASA 2003) – sample with a spectrophotometer. Small particles may be left in the water after filtering (e.g. Aas 2000), resulting in too high a_{CDOM} and an error in the estimation of S_{CDOM}. Several methods for correcting for this residual scattering have been proposed (Bricaud et al. 1981, Green & Blough 1994, Stedmon et al. 2000). Detritus mainly absorbs radiation and usually exponential increase with a decreasing wavelength analogous to that with CDOM is assumed (Roesler et al. 1989). The slope of detritus absorption is usually lower than that of a_{CDOM} (Roesler et al. 1989, Strömbeck 2001).

Pigments in phytoplankton can be divided into chlorophylls (*a*, *b* and *c*), biliproteins (phycocyanin and phycoerythrin) and carotenoids, each with one or more specific absorption peaks (Rowan 1989). In addition, phytoplankton contains decomposed pigments, such as phaeophytin *a*, a degradation product of chlorophyll *a*. Chlorophyll *a* has two absorption peaks, centred at about 440 and 675 nm and is present in all phytoplankton groups. The specific pigments of phytoplankton groups, such as phycocyanin of cyanobacteria with an absorption peak at about 620 nm, mean that the phytoplankton groups can have characteristic absorption spectra. This enables distinguishing phytoplankton groups from measured reflectance spectra (Gege 1998). Promising results have been reported particularly for cyanobacteria estimation from measured reflectance in eutrophic-hypertrophic lakes (Dekker 1993, Simis et al. 2007).

Absorption by phytoplankton, $a_{ph}(\lambda)$ and tripton, $a_{tri}(\lambda)$, can be measured in the laboratory with the filter pad method, using a spectrophotometer and an integrating sphere (Ferrari & Tassan

1999, Tassan & Ferrari 2002). Specific a_{ph} (a^*_{ph}) decreases with increasing biomass, because of the package effect and sometimes systematic changes in relationships between species breakdown/pigmentation and trophic level (Bricaud et al. 1995). Average $a^*_{ph}(\lambda)$ that takes into account the package effect has been presented for ocean waters (Bricaud et al. 1995), the Baltic Sea (Stahr & Markager 2002) and lakes (Strömbeck 2001, Reinart et al. 2004).

The specific backscattering coefficient of phytoplankton can vary between phytoplankton species (e.g. Ahn et al. 1992, Stramski et al. 2004) as a result of the variations in size, shape and refractive index of phytoplankton cells (e.g. Mobley 1994). In the Baltic Sea, specific backscattering has been observed to vary considerably between cyanobacteria species (Metsamaa et al. 2006).

Measurement of volume scattering and backscattering is more demanding than that of absorption (e.g. Vaillancourt et al. 2004). As a consequence, direct measurements of $b_{b,ph}$ in lakes are few and the estimation of backscattering properties of phytoplankton in bio-optical modelling of lakes (Kutser 1997, Strömbeck 2001, Dall'Olmo & Gitelson 2006) has mainly been based on research results for ocean phytoplankton or on theoretical simulations. Backscattering by inorganic particles in lakes has been reported to increase with decreasing wavelength (Bukata et al. 1991, Gallie & Murtha 1992, Strömbeck 2001) and has been described in bio-optical models by a power function (Bukata et al. 1991, Strömbeck 2001).

Inelastic (trans-spectral) processes in natural waters include Raman scattering by pure water and fluorescence. Fluorescence is generated by phytoplankton pigments (e.g. chlorophyll *a* with emission centred at about 685 nm and phycoerythrin with emission centred at about 585 nm). CDOM produces broad fluorescence, which peaks at blue wavelengths. Fluorescence can influence reflectance spectrum in lakes and coastal waters, if phytoplankton or CDOM concentration is high and mineral particle concentration is low (Bukata et al. 2004).

1.2.2 Remote sensing and reflectance modelling

The water-leaving radiance carries information on scattering and absorption coefficients – and, consequently, on the concentrations of CPSs. However, the water leaving component is only a small amount of the radiance measured by a satellite instrument; the rest is mainly due to atmospheric effects. An important part of remote sensing is correction of the measured radiance for atmospheric effects and other confounding factors, such as the adjacency effect (some of radiation from land pixels reaches the instrument such that it appears to come from water pixels). The adjacency effect can affect water pixels up to several kilometres from shore (Santer & Schmechtig 2000).

The radiance measured by a remote sensing sensor (assuming no adjacency effect or reflection from the bottom) can be expressed as

$$L_{inst}(\theta_v, \phi_v, \theta_s) = L_r(\theta_v,\phi_v,\theta_s) + L_a(\theta_v,\phi_v,\theta_s) + T_{atm}(\theta_v,\theta_s)\, L_{surf}(\theta_v,\phi_v,\theta_s) \quad (7)$$

where L_{inst} is radiance measured at the instrument, L_r is radiance due to Rayleigh scattering by air molecules, L_a is radiance due to aerosol scattering, T_{atm} is atmospheric transmission factor, L_{surf} is surface radiance, θ_v is zenith observation angle, θ_v is azimuth observation angle θ_s and is solar zenith angle. T_{atm} depends on ozone content, Rayleigh scattering by air molecules, and scattering and absorption by aerosols.

L_{surf} can be estimated from L_{inst} by the application of atmospheric correction. The radiative-transfer-model-based atmospheric correction methods typically require information on the atmosphere – e.g. the ozone content and water vapour content, the surface pressure and the aerosol characteristics (e.g. Rahman & Dedieu 1994).

Water leaving radiance, L_w, can be calculated from L_{surf} by taking into account the blue-sky radiation reflected by the water surface (assuming that sun glint does not exist)

$$L_w(\theta_v,\phi_v,\theta_s)0 = L_{surf}(\theta_v,\phi_v,\theta_s) - \sigma_L\, L_{sky}(\theta_v,\phi_v,\theta_s) \quad (8)$$

where $L_{sky}(\lambda)$ is the average radiance of that area of the sky that is specularly reflected into the sensor. σ_L is the Fresnel reflectance and depends on the angle of reflection. It can be calculated, for example, from θ_v by means of the Fresnel equation (Jerlov 1976).

Remote sensing reflectance R_{rs} (sr^{-1}), which is also called water leaving reflectance, is defined as (e.g. Mobley 1994)

$$R_{rs}(\lambda,\theta_v,\phi_v,\theta_s) = \frac{L_w(0+,\lambda,\theta_v,\phi_v,\theta_s)}{E_d(0+,\lambda)} \quad (9)$$

where L_w is upwelling radiance ($W\ m^{-2}\ s^{-1}\ sr^{-1}$) in the instrument observation direction after removal of radiation reflected at the air-water-interface, E_d is downwelling irradiance ($W\ m^{-2}\ s^{-1}$) and 0+ refers to above-water observation.

Subsurface irradiance reflectance R at depth z_i is defined as

$$R(z_i,\lambda) = \frac{E_u(z_i,\lambda)}{E_d(z_i,\lambda)} \quad (10)$$

where E_u is upwelling plane irradiance and E_d is downwelling plane irradiance.

Remote sensing reflectance can be approximated from R (without angle dependencies) as follows (Mobley 1994):

$$R_{rs}(\lambda) = \frac{s}{Q} R(\lambda) \quad (11)$$

where s is the radiance reduction factor due to internal reflection and refraction at water-air interface. Q is the Q factor, which is the ratio between upwelling irradiance and radiance and has been reported to range mainly between 3 and 6 sr (e.g. Morel & Gentili 1996, Loisel & Morel 2001). Q factor depends e.g. on the zenith angle of the sun and the scattering phase function.

Reflectance models are standard tools in the remote sensing of water, utilised e.g. in sensitivity analyses and interpretation of water quality by inverse techniques. A widely used approximation in the calculation of irradiance reflectance just beneath the water surface (R) is (Gordon et al. 1975, simplified by Jerlov 1976)

$$R\ (0-,\lambda) = C\frac{b_{b,Tot}(\lambda)}{a_{Tot}(\lambda)+b_{b,Tot}(\lambda)} \quad (12)$$

where C depends mainly on the illumination conditions. Also more physically based reflectance models are available, such as Hydrolight (Mobley 1994, Mobley & Sundman 2007), which is based on the radiative transfer equations. Hydrolight calculates radiance distributions and derived optical quantities, and considers their in depth variations.

1.2.3 Diffuse attenuation coefficient

The diffuse attenuation coefficient for downward irradiance, K_d, is defined as

$$K_d(z,\lambda) = \frac{1}{z_2 - z_1} \ln\left[\frac{E_d(z_2,\lambda)}{E_d(z_1,\lambda)}\right] \quad (13)$$

where z is water depth and E_d is downwelling plane irradiance.

Attenuation depth $z_{att}(\lambda)$ is

$$z_{att}(\lambda) = \frac{1}{K_d(\lambda)} \tag{14}$$

$z_{att}(\lambda)$ defines the depth of the surface layer represented by the remotely sensed estimates: about 90% of the backscattered light from a water column to the atmosphere comes from the surface layer down to z_{att}.

1.2.4 Interpretation of water quality from remote sensing data

The ideal case in the interpretation of water quality from remote sensing data would be for the CPS of interest to have a clear optical signature (absorb, scatter or emit light) in a wavelength region where other CPSs do not affect reflectance. Natural waters, however, are usually far from the ideal case and the wavelength regions of the optical signatures of different CPSs often overlap each other.

The main approaches in the interpretation of water quality from remote sensing data are semi-empirical and semi-analytical algorithms. In semi-empirical algorithms, channels or channel ratios are selected on the basis of knowledge of the optical properties of CPSs and their impact on the reflectance spectrum. This knowledge is used in analyses of remote sensing data by focusing on those channels where the CPS of interest has its optical signature and the effect of other CPSs is minimal, or their impact on the reflectance at the applied channels can be estimated. Semi-empirical algorithms usually require simultaneous *in situ* data for algorithm training and are often image-dependent.

In semi-analytical algorithms, remote sensing data are corrected for atmospheric and other confounding factors to get R_{rs} or R. CPSs are obtained through inversion of a reflectance model. The problem of long computing time due to pixel-by-pixel inversion of remote sensing data has been solved through the use of neural networks (e.g. Schiller & Doerffer 1999), matrix inversion (Hoge & Lyon 1996) and Levenberg Marquardt multivariate procedure (e.g. Pozdnyakov et al. 2005, Van Der Woerd & Pasterkamp 2008).

The most common optical classification in remote sensing and optics of natural waters is the Case 1 – Case 2 scheme, first presented by Morel and Prieur (1977) and modified by Gordon and Morel (1983) and Morel (1988). Clear ocean waters are optically classified as Case 1 waters, where phytoplankton with its covarying material of biological origin is the principal CPS responsible for the variation in optical properties. In Case 1waters, the contribution of CPSs other than phytoplankton is small and they can be modelled as a function of phytoplankton concentration. For these reasons, semi-empirical algorithms based on the blue/green channel ratio have been successful in the estimation of chlorophyll *a* in ocean waters (e.g. O'Reilly et al. 1998). Lakes and coastal waters usually are among Case 2 waters, where other substances (CDOM and inorganic particles) in addition to phytoplankton may make a significant contribution to optical properties and they can vary independently of phytoplankton. Mobley et al. (2004) suggested dropping the Case 1 – Case 2 classification and focusing on optical modelling of water according to whatever CPSs are present. Nevertheless, the Case 1 – Case 2 scheme is still useful in explaining the basic optical complexity of Case 2 waters in comparison to most ocean waters, which were the starting point of aquatic optics.

1.3 Objectives

In lake-rich regions, only a small proportion of the lakes belong to the monitoring network. In Finland, for example, lakes larger than 0.01 km^2 number 56,012 (Raatikainen & Kuusisto 1988); about 4% of them are monitored annually (**PVI**). Because of the good spatial coverage, remote sensing could improve the effectiveness of lake monitoring by providing information on all lakes in an image, spatial differences within a lake and temporal variation in water quality.

One of the main water quality problems in lakes is eutrophication, which is often measured in terms of chlorophyll *a* concentration in routine monitoring programmes and which can be estimated via remote sensing. In the Water Framework Directive (WFD, European Union 2000), ecological classification of lakes is based on the four biological elements: phytoplankton, other aquatic flora, benthic invertebrates and fish. Only about 10% of the WFD lakes in Finland (mainly having area > 0.5 km^2) could be classified by means of the available biological elements (Vuori 2009). In all, 59% of the 4275 lake waterbodies of WFD reported to EU in 2010 missed ecological classification or other status estimation (Ministry of the Environment 2011). This calls for new methods for the mapping of a large number of lakes. Some of the lakes missing biological measurements were assessed on the basis of the physico-chemical elements (mainly chlorophyll *a*).Thus chlorophyll *a* measurements, as a measure of phytoplankton biomass, support WFD reporting.

Turbidity and transparency can be used e.g. to estimate the spreading of agricultural river loading in lakes. Transparency in WFD is defined as one of the supporting variables to the biological elements. Humic (CDOM) level is one of the main criteria in the characterisation of surface water body types in WFD in Finland. In an end-user survey on the use of water remote sensing in Finland (Anttila et al. 2005), chlorophyll *a* and Secchi disk transparency (Z_{SD}) were considered the most useful among the water quality variables that potentially can be estimated by remote sensing.

Lake mapping on a global scale could have important applications in fields such as climate change studies. Lakes are commonly ignored in global estimates of carbon budgets (IPCC 2001), although they play an active role in the global carbon cycle (Downing et al. 2006, Cole et al. 2007). Estimation of the dissolved organic carbon (based on CDOM) in lakes by means of satellite remote sensing could be an aid in assessment of the carbon pool and its variation in lakes and in estimating CO_2 efflux from lakes.

The main objective of this study was to investigate and test remote sensing interpretation algorithms for water quality estimation in Finnish lakes, which represent boreal lakes with a wide range of CDOM variation. Another major objective was to develop optical models for the needs of interpretation and for the estimation of light attenuation. In addition, the work aimed at demonstrating the advantages of the use of remote sensing as compared to the conventional monitoring methods. The work focused on optically deep waters.

In detail, the individual objectives were to

- obtain information on the variation of colour-producing substances (CPS) and apparent optical properties in Finnish lakes,
- determine specific inherent optical properties and develop optical models for Finnish lakes,
- develop and test interpretation algorithms for the estimation of water quality in Finnish lakes by using semi-empirical and semi-analytical methods,
- investigate the applicability of channel configurations of different satellite instruments for water quality (CPS and Secchi disk transparency) estimation,
- investigate whether water quality can be estimated by satellite instruments (ETM+ and MERIS) with reasonable accuracy without image-specific algorithm training with *in situ* data and

- quantitatively compare the spatial information obtained via remote sensing to information collected through discrete sampling of routine lake monitoring

The first investigation of airborne remote sensing that used a large dataset (**PIII**) pointed up the complexity of water quality interpretation. This led to the investigation of SIOPs, CPS variations and their effects on reflectance (**PI** and **PII**). Knowledge of the SIOPs drew the author's interest to other AOPs – namely, spectral K_d and Z_{SD} – and their modelling (**PII**). The final objective of remote sensing is to produce valuable information for the needs of monitoring. Large-scale remote sensing for lakes is, in practice, possible only with satellite instruments, which were included in the algorithm studies of satellite images (**PV**, **PVI** and unpublished results) and in channel configuration analyses (**PI**). The production of remote-sensing-based water quality maps led to quantitative investigations of accuracy improvements obtained by means of spatial data (**PV** and **PVI**). The contents of **PI**–**PVI** are summarised in Figure 1.

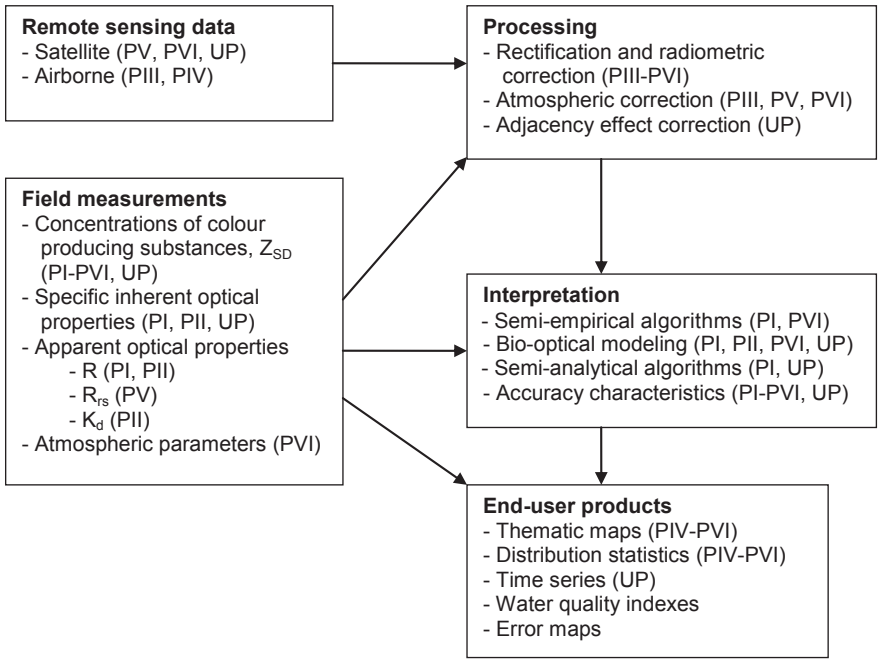

Figure 1. The main elements of remote sensing of water quality and how the original publications (PI–PVI) and unpublished investigations (UP) relate to them.

2 Material and methods

The experimental material for this thesis comprised three dataset levels: detailed optical measurements in a few lakes, remote sensing measurements with concurrent *in situ* sampling and automatic raft measurements, and a national dataset of routine measurements of CPSs and Z_{SD} (Table 1). These datasets made it possible to test and develop optical models and to investigate semi-empirical and inversion-based interpretation methods for different lake types. Joint use of the optical models and the national dataset enabled the investigation of optical properties and interpretation algorithms in highly varying combinations of CPSs.

Table 1. The main characteristics of the datasets and measurements.

Data	Measurements	No of lakes/ observations	Location	Main purpose	Publications
National	CPS and Z_{SD}	1113/3549	Whole Finland	Distribution of CPS and Z_{SD} in Finnish lakes	PII
Optical	E_{DW} and E_{UW} (LI-1800UW), a_{tot} and b_{tot} (ac-9), $a_{cdom}(\lambda)$	11/20	Southern and northern Finland	SIOPs, reflectance model, K_d- and Z_{SD}-models, interpretation of CPS by semi-analytical algorithm	PI, PII
Airborne	AISA	11/127	Southern Finland	Semi-empirical algorithms, comparison with discrete water quality information in single lakes	PIII, PIV
Satellite	ETM+, ALI	52/78	Karjaanloki and Siuntionjoki river basins, Southern Finland	Semi-empirical algorithms, comparison with discrete water quality information in river basin scale	PV, PVI
	MERIS	3/see text	Lake Pyhäjärvi, Vesijärvi and Päijänne	Semi-analytical algorithm, time series,	UP

2.1 Study sites and datasets

The national dataset was obtained from the Environmental Information System of the Finnish Environment Administration and covered the period July–August in 2000–2002. This dataset, consisting of 3,549 observations, from 1,670 stations (Figure 2), was used to 1) calculate CPS and Z_{SD} distributions, 2) calculate K_d(PAR) and attenuation depth distributions with the aid of a $K_d(\lambda)$ model and 3) investigate semi-empirical algorithms based on the simulated $R(\lambda)$.

Most Finnish lakes are oligo- or mesotrophic and the CDOM concentration can be high (Table 2). The correlations between C_{TSS}, $C_{Chl\text{-}a}$, $a_{CDOM}(400)$ and Z_{SD} in the whole dataset were low (correlation coefficient < 0.48) with the exception of C_{TSS} vs. $C_{Chl\text{-}a}$ (correlation coefficient = +0.64) and $a_{CDOM}(400)$ vs. Z_{SD} (-0.57).

Table 2. Statistical characteristics of CPSs and Z_{SD} in the national dataset and also K_d(PAR) and maximum z_{att}, calculated via the K_d model from station mean values in the dataset (**PII**) (P10 = 10th percentiles and P90 = 90th percentiles).

	P10	Median	P90	Mean	Min	Max	N
C_{TSS} (mg l^{-1})	0.7	2.20	9.3	4.3	0.19	151	3549
$C_{Chl\text{-}a}$ (µg l^{-1})	2.8	9.8	41.2	18.3	0.5	450	3549
$a_{cdom}(400)$ (m^{-1})	2.1	7.4	19	8.9	0.6	74	3549
Z_{SD} (m)	0.75	1.8	4.0	2.1	0.1	11	3549
$K_d(PAR)$ (m^{-1})	0.90	2.75	6.7	3.46	0.374	28.6	1670
Max Z_{att} (m)	0.45	1.05	2.20	1.23	0.06	5.55	1670

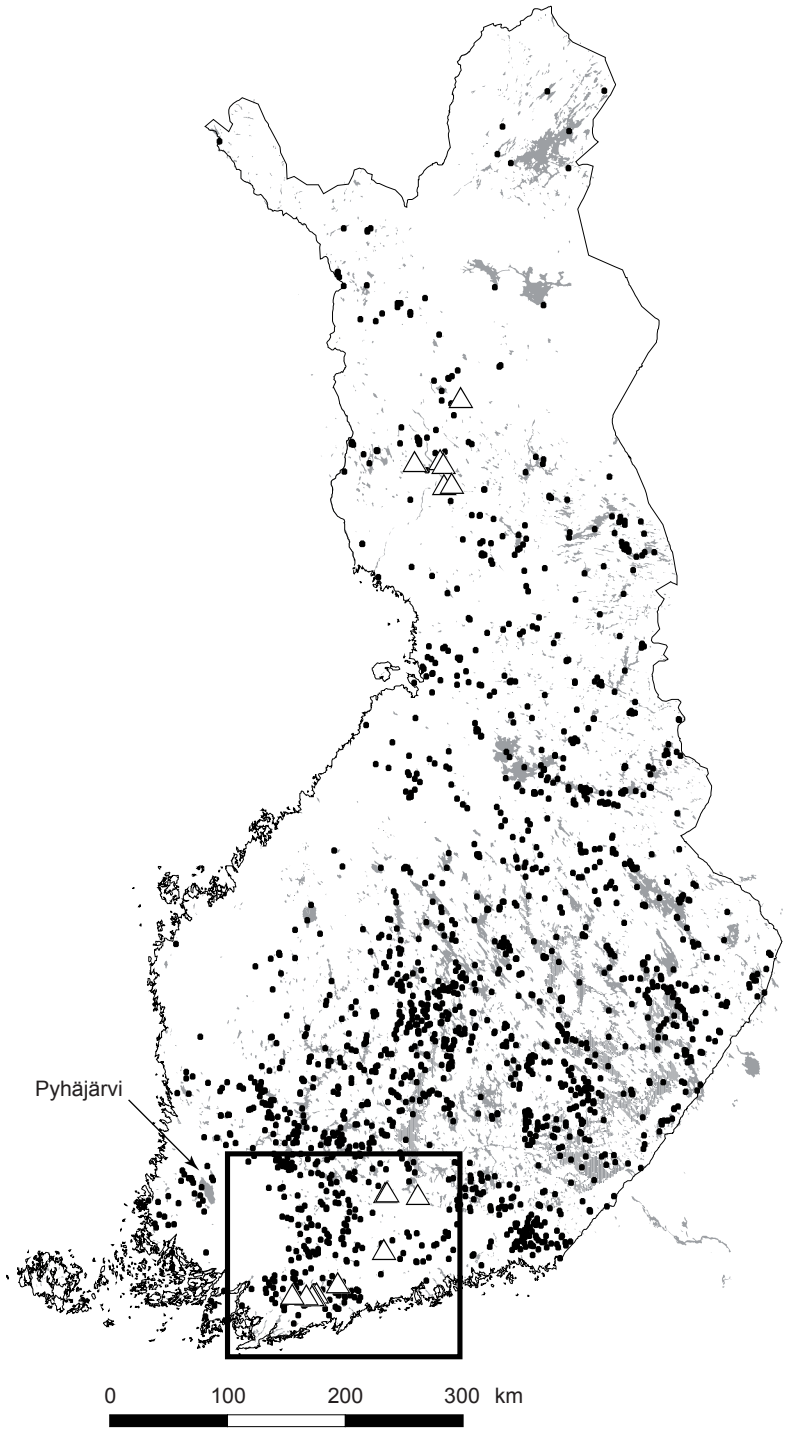

Figure 2. Location of stations of the national dataset (•) and the optical measurements of this study (Δ). The AISA, ETM+ and ALI studies took place in the area indicated by a rectangle (see Figure 3). Grey areas are lakes. Lake Pyhäjärvi was included in the MERIS study (**UP**). Background map: © National Land Survey of Finland, license no. 7/MYY/06.

Optical measurements were carried out in 1997 and 1998 at 11 lakes, in southern and northern Finland (Figure 2). Details on the optical dataset are presented in the appendix. The AISA airborne spectrometer measurements consisted of four surveys in southern Finland: August 1996, May 1997, August 1997 and August 1998 (Figure 3). The spatial distribution of chlorophyll *a*, based on AISA data, was analysed in two lakes, Hiidenvesi and Lohjanjärvi (**PIV**).

The Landsat ETM+ and EO-1 ALI studies included two river basins, Karjaanjoki (A = 2,046 km^2) and Siuntionjoki (A = 487 km^2); see Figure 3. The three Landsat 7 ETM+ images from 2002 were acquired on 20 May, 16 July and 9 September. The *in situ* observations used in combination with ETM+ images consisted of 1) water sampling in Lake Lohjanjärvi on the days the Landsat satellite passed above, 2) turbidity measurements with the TPS WP89 portable meter at 27 locations in Lake Lohjanjärvi on 9 September 2002, 3) volunteer Z_{SD} measurements on the Landsat overflight days and 4) routine lake water sampling in the river basins within three days of the Landsat overflight (**PVI**). The EO-1 ALI image was acquired on 14 July 2002, covering an area of 37 x 185 km in the Karjaanjoki river basin and its surroundings. *In situ* measurements of the ALI investigations were made in 13 lakes on 14–17 June 2002. The ALI data was used only for CDOM estimation (**PV**).

The MERIS dataset consisted of 21 cloudless images acquired at Lake Pyhäjärvi (Figure 2) in 2009 and three images in 2007 in Lakes Pyhäjärvi, Vesijärvi and Päijänne (Figure 3). The MERIS estimates were compared with water quality measurements of the automatic raft station of Lake Pyhäjärvi and with ac-9 transects in these three lakes.

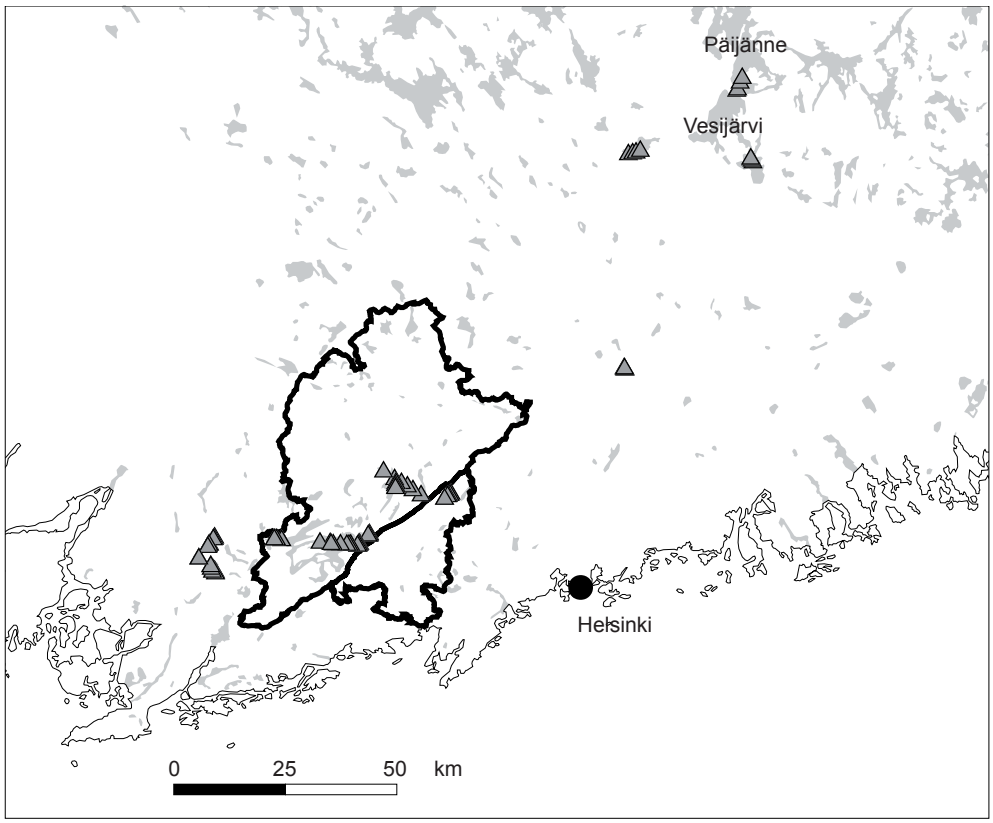

Figure 3. Location of the *in situ* sampling stations (grey triangle) of the AISA measurement campaigns and the borders of the Karjaanjoki and Siuntionjoki river basins, which were included in the ETM+(**PVI**) and ALI (**PV**) studies. Grey areas are lakes. Lakes Vesijärvi and Päijänne were included in the MERIS study (**UP**). For the orientation in Finland, see Figure 2. Background map: © National Land Survey of Finland, license no. 7/MYY/06.

2.2 Water quality determinations

The concentration of total suspended solids (C_{TSS}) was determined in laboratory by means of gravimetric determination of the matter removed by a filter (EN 872, Nuclepore polycarbonate 0.4 µm filter). The concentration of the sum of chlorophyll *a* and phaeophytin *a* ($C_{Chl\text{-}a}$) was measured with a spectrophotometer after extraction with hot ethanol (ISO 10260, GF/C filter). Turbidity (Turb, measured in FNUs) was determined by the nephelometric method (EN 27027, based on measurement of light (860 nm) scattered within a 90° angle from a beam directed at the water sample, with formazine used as a standard matching solution). a_{CDOM} was measured for the 400–750 nm (see next section) and $a_{CDOM}(400)$ was selected for a measure of the CDOM concentration.

In routine water quality monitoring in Finland, the concentration of humic substances is indirectly determined via the 'water colour' (mg Pt l^{-1}) method, which is based on the comparison of water samples with standard cobalt chloride disks (ISO 7887 1994). For the needs of the optical models, Pt water colour in the national dataset was converted to $a_{CDOM}(400)$ with $a_{CDOM}(400)$ = 0.123 * colour (R^2 = 0.83, N = 449, $a_{CDOM}(400)$ range: 0.1–34 m^{-1}, **PII**). In addition, C_{TSS} was estimated from turbidity in the national dataset with C_{TSS} = 1.162 * *Turb* (R^2 = 0.82, N = 106, C_{TSS} range: 0.4–17 mg l^{-1}, **PII**).

The CPS determinations were made in the water laboratory of Western-Uusimaa Water and Environment Ltd; the water laboratory of the Finnish Environment Institute; and the Uusimaa, Lapland and South-west Regional Environment Centres. In addition, the national CPS and Z_{SD} data included the results from national and regional monitoring carried out by all regional environment centres in Finland and via local statutory monitoring. Water samples were taken from depths of 0.2 (AISA) and 1.0 m (ETM+, national dataset) and from 0.2 and 1.0 m depths (optical dataset). In the national and ETM+ datasets, $C_{Chl\text{-}a}$ was determined from a composite sample of 0–2 m.

Turbidity at the automatic raft station of Lake Pyhäjärvi was measured with nitro::lyser (s::can) and $C_{Chl\text{-}a}$ with a microFlu-chl unit (TriOS) at one-hour intervals. After the measurement period, the automatic measurements were corrected by way of the results for the control samples, which were analysed in the laboratory of the Water Protection Association of Southwestern Finland. Estimations of *in situ* a_{CDOM} for the MERIS overflight dates were interpolated from the routine monitoring measurements (six measurements in 2009). The raft, automatic instruments and data are described in detail by Kallio et al. (2010).

2.3 Optical measurements

The optical measurements conducted in field consisted of upwelling and downwelling plane irradiances (LI-1800UW underwater spectrometer, LI-COR) and total absorption and attenuation coefficients (ac-9 absorption/attenuation meter with an optical path length of 25 cm, from WET Labs, Inc.). R was calculated from the E measurements according to Equation 10.

The wavelengths used with the ac-9 absorption/attenuation meter were 412, 440, 488, 510, 532, 555, 650, 676 and 715 nm. The measurements were corrected for temperature and scattering according to the ac-9 manual (WET Labs 1995). In the further analyses of the data, the average values of the measurements taken from 0–2 m were used. The measurement protocols and the data processing of the ac-9 and LI-1800UW are described in detail in **PI**. The measurement technique for the ac-9 transects in the validation of MERIS images in Lakes Pyhäjärvi, Vesijärvi and Päijänne was the same as in the work of Lindfors et al. (2005).

The absorption spectra (380–800 nm) of CDOM were measured with a spectrophotometer (cuvette length of 50 mm in most cases but in a few cases 10 mm) from a sample filtered through a Nuclepore polycarbonate 0.4 µm filter. The absorption measurements were corrected for residual scattering by subtracting absorption at 750 nm from the measured values in 400–750 nm (Green & Blough 1994).

2.4 Bio-optical models

This study included optical models for the calculation of $R(\lambda)$, $K_d(\lambda)$ and Z_{SD}. Similar models have been widely used in water optics and remote sensing, but the models had to be parameterised and tested in the lakes under investigation. An additional aim here was to investigate the models' performance in CDOM-rich waters with varying $C_{Chl\text{-}a}$ and C_{TSS}. The *R* model was used to investigate 1) the effect of CPS variations on the interpretation of CPSs (**PI** and **PVI**), 2) the sensitivity of S_{CDOM} variation interpretation of CPSs by semi-empirical algorithms (**PII**) and 3) interpretation of CPSs by the inversion method (**PI**). All of the models applied require SIOPs, which were measured at the optical stations or taken from other studies performed in Finnish lakes.

2.4.1 Absorption and scattering

The total absorption ($a_{tot}(\lambda)$) and scattering ($b_{tot}(\lambda)$) coefficients, needed in the $R(\lambda)$, $K_d(\lambda)$ and Z_{SD} models, were calculated from SIOPs and CPS concentrations. The $R(\lambda)$ model additionally requires backscattering ratios for the calculation of $b_{b,tot}(\lambda)$.

The bio-optical models of this study assume, in addition to pure water, three colour-producing components: phytoplankton, tripton and CDOM (Equation 1). The calculation of the components of $a_{tot}(\lambda)$ is described by equations 15–18.

Absorption by CDOM was calculated by assuming an exponential increase with a decreasing wavelength (Bricaud et al. 1981):

$$a_{cdom}(\lambda) = a_{cdom}(400)\, e^{-S_{cdom}(\lambda - 400)} \tag{15}$$

where $a_{CDOM}(400)$ is the absorption coefficient of CDOM at 400 nm and S_{CDOM} is the spectral slope coefficient.

Absorption by phytoplankton, $a_{ph}(\lambda)$, was calculated by

$$a_{ph}(\lambda) = a^*_{ph}(\lambda) C_{Chl-a} \tag{16}$$

where $a^*_{ph}(\lambda)$ is the *Chl-a* specific absorption coefficient of phytoplankton.

Absorption by tripton, $a_{tri}(\lambda)$, was expressed as:

$$a_{tri}(\lambda) = a^*_{\underline{TSS}}(\lambda) C_{TSS} \tag{17}$$

where $a^*_{\underline{TSS}}(\lambda)$ is the specific absorption of bleached (pigments were broken down in order to exclude a_{ph}) total suspended solids. C_{TSS} is the concentration of TSS. Absorption by tripton was defined by means of C_{TSS}, because tripton concentration measurements were not available. $a^*_{\underline{TSS}}(\lambda)$ was described analogously to the calculation of $a_{CDOM}(\lambda)$ (Roesler et al. 1989):

$$a^*_{\underline{TSS}}(\lambda) = a^*_{\underline{TSS}}(400)\, e^{-S_{Tri}(\lambda - 400)} \tag{18}$$

where $a^*_{\underline{TSS}}(400)$ is the specific absorption of bleached total suspended solids at 400 nm and S_{tri} is the spectral slope coefficient of tripton absorption.

The total scattering coefficient, $b_{tot}(\lambda)$, was calculated as:

$$b_{tot}(\lambda) = b_w(\lambda) + b^*_{TSS}(\lambda)C_{TSS} \quad (19)$$

where $b_w(\lambda)$ is the scattering coefficient of pure water and $b^*_{TSS}(\lambda)$ is the specific scattering coefficient of the TSS.

The specific scattering coefficient of TSS ($b^*_{TSS}(\lambda)$) was described by a power function (e.g. Jupp et. al. 1994, Strömbeck 2001):

$$b^*_{TSS}(\lambda) = b^*_{TSS}(555)\left(\frac{555}{\lambda}\right)^{n_b} \quad (20)$$

where $b^*_{TSS}(555)$ is the specific scattering coefficient of TSS at 555 nm and n_b is the scattering exponent.

The total backscattering coefficient, $b_{b,tot}(\lambda)$, needed in the reflectance model (Equation 12), is described by:

$$b_{b,tot}(\lambda) = \hat{b}_{bw} b_w(\lambda) + \hat{b}_{b,TSS} b^*_{TSS}(\lambda) C_{TSS} \quad (21)$$

where $\hat{b}_{bw}$ and $\hat{b}_{b,TSS}$ are the backscattering ratios of pure water and TSS, respectively. $\hat{b}_{b,TSS}$ was assumed to be independent of wavelength (Whitmire et al. 2007).

2.4.2 Reflectance model and inversion

The irradiance reflectance just beneath the water surface, $R(\lambda)$,was calculated according to Equation 12. Inelastic processes were not considered in the reflectance model. Inelastic processes have been included in a few reflectance models of lakes (e.g. Grassl et al. 2002), but their modelling is more demanding than in case of elastic processes. The C in Equation 12 comprises the illumination dependencies and was estimated according to Kirk (1984):

$$C = -0.629\mu_0 + 0.975 \quad (22)$$

where μ_0 is the cosine of the solar zenith angle in the water.

The inversion-based interpretation algorithm applied to the measured R at the optical stations relied on the maximum-likelihood method, assuming that the forward (reflectance) modelling error is normally distributed. Following this, the maximum-likelihood estimate for multiple variables was obtained by finding the maximum value of a multidimensional Gaussian conditional probability density distribution. When the modelling errors of different channels are assumed to be independent from each other, the constrained minimisation problem obtained for the joint estimation of C_{TSS}, $C_{Chl\text{-}a}$ and $a_{CDOM}(400)$ was (with respect to constrains: $0.2 \leq C_{TSS} \leq 25$ mgl^{-1}, $0.2 \leq C_{Chl\text{-}a} \leq 100$ µgl^{-1}, $0.2 \leq C_{TSS} \leq 25$ mgl^{-1})

$$\min_{\mathrm{TSS,\,Chl-a,\,a400}} \sum_{i=1}^{n} \frac{1}{2\sigma_i^2}\left(R_{\mathrm{i,sim}} - R_{\mathrm{i,mea}}\right)^2 \quad (23)$$

where σ_i is the standard deviation of statistical reflectance modelling error for channel i. $R_{i,sim}$ and $R_{i,mea}$ are the simulated and measured reflectance for channel i, respectively. σ_i was estimated by using the root mean squared error (RMSE), which was calculated from the residual errors between the measured and simulated reflectances. R_{sim} in Equation 23 was calculated by means of Equation 12, utilising Equations 1, 21 and 22. The components of a_{tot} and $b_{b,tot}$ were obtained via Equations 15–20. In practice, each inversed squared variance term, σ_i^{-2}, weighted each channel according

to its estimated modelling accuracy. Inversion analyses were performed for the full spectrum and for each channel of the ETM+, MODIS and MERIS instruments (Table 3) constructed from the measured $R(\lambda)$.

Table 3. Channel configuration of the ETM+, ALI, MODIS (1,000 m data) and MERIS satellite instruments in the 400–760 nm range, with the spatial resolution indicated under the instrument name (**PI**).

Channel number	Wavelength range (nm)			
	ETM+ 25 m	ALI 25 m	MODIS 1,000 m	MERIS 300 m
1	450–520	450–515	405–420	407.5–417.5
2	530–610	525–605	438–448[1]	437.5–447.5[1]
3	630–690	630–690	483–493	485–495
4			526–536	505–515
5			546–556	555–565
6			662–672	615–625
7			673–683	660–670
8			743–753[2]	677.5–685
9				703.75–713.75[3]
10				750–757.5[2]

[1] 450–460 nm in the subsurface reflectance study (**PI**)
[2] 743–750 nm in the subsurface reflectance study (**PI**)
[3] 700–710 nm in the subsurface reflectance (**PI**)

2.4.3 K_d and Z_{SD} models

The mean $K_d(\lambda)$ in the euphotic zone can be estimated with (Kirk 1984):

$$K_d(\lambda) = \frac{1}{u_0}\left(a_{Tot}(\lambda)^2 + (g_1 u_0 - g_2)\, b_{Tot}(\lambda)\, a_{Tot}(\lambda)\right)^{\frac{1}{2}} \quad (24)$$

where u_0 is the cosine of the solar zenith angle in the water. Coefficients g_1 and g_2 depend on the shape of the scattering phase function. Here, $g_1 = 0.425$ and $g_2 = 0.190$ were used as proposed by Kirk (1984), who applied the scattering phase function of Petzold (1972).

The other tested $K_d(\lambda)$ model was (e.g. Maffione & Jaffe 1995, Herlevi 2002):

$$K_d(\lambda) = D_1 \cdot a_{Tot}(\lambda) + D_2 \cdot b_{Tot}(\lambda) \quad (25)$$

where D_1 and D_2 are empirical coefficients.

Z_{SD} was modelled according to Tyler (1968):

$$Z_{SD} = C_2 \frac{1}{c_{Tot}(PAR) + K_d(PAR)} \quad (26)$$

where C_2 is an empirical coefficient, $c_{tot}(PAR)$ is the total beam attenuation coefficient of the PAR (400–700 nm) region of the spectrum and $K_d(PAR)$ is the diffuse attenuation coefficient of PAR.

Z_{SD} was also calculated with a simplified version of Equation 26 presented by Höjerslev (1986, ref. Preisendorfer 1986):

$$Z_{SD} = C_1 \frac{1}{c_{Tot}(PAR)} \quad (27)$$

where C_1 is an empirical coefficient. Estimation of the empirical coefficients in Equations 25–27 is described in section 2.4.4.

2.4.4 Estimation of coefficients for the optical models

The *Chl-a* specific absorption coefficient of phytoplankton, a^*_{Ph}, in Equation 16, was calculated via the power function originally presented by Bricaud et al. (1995):

$$a^*_{Ph}(\lambda) = A(\lambda) C_{Chl}^{-B(\lambda)} \quad (28)$$

where $A(\lambda)$ and $B(\lambda)$ are positive empirical coefficients. Here $A(\lambda)$ and $B(\lambda)$ were obtained from a study by Ylöstalo (unpublished), carried out in 2000 and 2002 at 10 Finnish lakes. $a^*_{TSS}(400)$)and S_{tri} were also from the study of Ylöstalo. S_{CDOM} was estimated by fitting Equation 15 to the measured $a_{CDOM}(\lambda)$ (18 spectra of the optical dataset, 400–750 nm wavelength region) (**PI**).

Scattering related IOPs ($b^*_{TSS}(\lambda)$, $b^*_{TSS}(555)$ and n_b, Equation 20) were estimated from the ac-9 and C_{TSS} measurements (**PI**). $b^*_{TSS}(\lambda)$) was calculated for the nine ac-9 wavelengths by

$$b^*_{TSS}(\lambda) = \frac{b_{Tot}(\lambda) - b_w(\lambda)}{C_{TSS}} \quad (29)$$

The backscattering ratio of TSS ($\hat{b}_{b,TSS}$) was estimated by fitting the modelled reflectance spectrum (Equations 12 and 21) with the 12 measured $R(\lambda)$. The 400–448 nm range was not included in the analyses, because of the difficulties in measuring the low irradiance levels and possible instrument self-shading, which has its greatest influence at the blue end of the spectrum (Gordon & Ding 1992).

The simple $K_d(\lambda)$ and Z_{SD} models were parameterised and tested with the optical dataset (**PII**). All optimised coefficients of the bio-optical models (S_{CDOM}, n_b, $\hat{b}_{bTSS}$ and the empirical coefficients of the K_d and Z_{SD} models) were determined with the least-squares method according to a Nelder–Mead simplex search technique (Nelder & Mead 1965).

2.5 Processing of the remote sensing data

The flight altitude of the AISA airborne imaging spectrometer (Mäkisara 1998) measurements ranged from 1,000 to 3,000 m. The channel combinations differed slightly between the surveys and 24 channels with approximately the same position and width (5–8 nm) were selected for the final analyses (**PIII**). A pixel size of 2 x 2 m was selected for the geometrically and radiometrically corrected AISA images. Before the comparison with *in situ* measurements, AISA data from an area of 20 x 20 m were averaged at each *in situ* sampling station. The AISA radiances were converted to reflectances through the atmospheric correction method developed by de Haan and Kokke (1996), which utilises the MODTRAN radiative transfer code simulations. The procedures applied and the configurations of the AISA are reported in detail in **PIII** and by Attila et al. (2008).

The three ETM+ images acquired in 2004 were rectified to national geographic co-ordinates on the basis of 25 ground control points and top-of-atmosphere (TOA) radiances were calculated (**PVI**). Atmospheric correction for the ETM+ images was conducted via the SMAC (Simplified Method of Atmospheric Correction) model (Rahman and Dedieu 1994). The estimation of the atmospheric parameters (aerosol optical depth (AOD) at 550 nm, humidity and ozone concentration) is described in **PVI**. For comparison of the ETM+ data and *in situ* measurements, all pixels within

a radius of 75 m (30 pixels) and with their centre in the pixel corresponding to the geographic co-ordinates of the *in situ* stations were extracted. The atmospheric correction for the ALI image was based on use of the ENVI FLAASH software and of the overlapping HYPERION image (**PV**).

The MERIS images were processed by the Boreal Lakes processor version 1.0.2 (Doerffer & Schiller 2008a, Doerffer & Schiller 2008b, Koponen et al. 2008a), which is partly based on the MERIS Case 2 algorithm (Doerffer & Schiller 2007). The Boreal Lakes processor is a plug-in module of the BEAM software (http://www.brockmann-consult.de/beam/) and consists of the atmospheric correction (which generates R_{rs}) and the Hydrolight bio-optical model (Mobley 1994, Mobley & Sundman 2007). The bio-optical model yields $a_{ph}(443)$, $b_{TSS}(443)$ and $a_{CDOM}(443)$. $C_{Chl\text{-}a}$ and C_{TSS} are obtained by means of conversion factors – i.e., the relationship between the concentrations and a_{ph} or b_{TSS} at 443 nm. The ICOL adjacency effect correction (version 1.0, Santer & Zagolski 2008), also a plug-in module of BEAM, was used as a pre-processing step. For each output variable a 3 x 3 MERIS pixel square with its centre pixel corresponding to the location of the automatic raft station was extracted and the median of these pixel values was used in the final analyses.

The SIOPs needed in the bio-optical model (Doerffer & Schiller 2008b) of the Boreal Lakes processor were from **PI**, with the exception of SIOPs related to particulate absorption (a^*_{ph} and a^*_{tri}), which were updated on the basis of a larger dataset (Ylöstalo et al. 2011) than was available in **PI**. The ranges of CPSs needed in training of the neural networks of the processor were based on the national dataset (**PII**).

2.6 Statistics

Statistical accuracy characteristics of the interpretation algorithms were determined by
- the coefficient of determination (R^2),
- root mean squared error (RMSE),
- relative RMSE (RRMSE) and
- bias.

In the case of one predictor variable, RMSE was defined as (Milton & Arnold 1995)

$$RMSE = \sqrt{\frac{1}{N-j}\sum_{i=1}^{N}(CPS_{Obs,i} - CPS_{Est,i})^2} \tag{30}$$

where N is the total number of observations in the dataset, $CPS_{Obs,i}$ is the observed *in situ* value and $CPS_{Est,i}$ is the estimated value; $j = 2$ if observations are used for training the algorithm, while $j = 0$ for an independent dataset. RRMSE is RMSE as a percentage of the mean observation.

Evaluation of the statistical accuracy of remote-sensing-based $C_{Chl\text{-}a}$ estimation and the *in situ* $C_{Chl\text{-}a}$ measurements at discrete monitoring stations in Lakes Hiidenvesi and Lohjanjärvi was based on the calculation of 95% confidence intervals, standard errors and observed errors (**PIV**). The confidence interval (M_S) for the estimated mean $C_{Chl\text{-}a}$ of the area under investigation (lake) was obtained by means of

$$M_S = t_{\alpha/2} \cdot S \cdot \sqrt{\frac{1}{n} + \frac{\left(\langle X \rangle - \langle X_{ref} \rangle\right)^2}{S_{xx}}} \tag{31}$$

where $t_{a/2}$ is a coefficient based on the T_{n-2} distribution. S is the RMSE for algorithm training data and n is the number of samples in the training dataset. $\langle X \rangle$ is the mean of remotely sensed $C_{Chl\text{-}a}$ over the entire study area and $\langle X_{ref} \rangle$ is the corresponding mean value for the algorithm training data. S_{xx} in Equation 31 is given by

$$S_{xx} = \sum_{i=1}^{n} \left(x_{ref,i} - \left\langle X_{ref} \right\rangle \right)^2 \tag{32}$$

where $x_{ref,i}$ is the measured $C_{Chl\text{-}a}$ for training data point i. The confidence intervals presented are the 95% bounds that indicate the limits within which the estimated mean is located with a probability of ≥ 95%.

The standard error (*SE*) of the $C_{Chl\text{-}a}$ estimates was presented for both *in situ* sampling and remote-sensing-data-based estimates. In the case of discrete *in situ* sampling, the *SE* of the estimated mean among sampling stations is

$$se_{\langle C_{Chl-a} \rangle} = \frac{s_{\langle C_{Chl-a,ref} \rangle}}{\sqrt{n}} = \sqrt{\frac{\sum_{i=1}^{n} \left(C_{Chl-a,ref,i} - \left\langle C_{Chl-a,ref} \right\rangle \right)^2}{n-1}} \cdot \frac{1}{\sqrt{n}} \tag{33}$$

where $\langle C_{chl,ref} \rangle$ is the mean $C_{Chl\text{-}a}$ of discrete sampling stations.

Accordingly, the SE for the remote-sensing-data-based estimate of the mean $C_{Chl\text{-}a}$ can be defined as

$$SE_{\langle C_{chl,AISA} \rangle} = S \cdot \sqrt{\frac{1}{n} + \frac{\left(\langle X \rangle - \left\langle X_{ref} \right\rangle \right)^2}{S_{xx}}} \tag{34}$$

The observed error (difference to the AISA based estimation) for the discrete data was obtained by

$$E_{\langle C_{Chl-a} \rangle} = \left| \left\langle C_{Chl-a,ref} \right\rangle - \left\langle C_{Chl-a,AISA} \right\rangle \right| \tag{35}$$

where $\left\langle C_{Chl-a,AISA} \right\rangle$ is the mean AISA-based estimate of $C_{Chl\text{-}a}$.

3 Results and discussion

This section presents the main results of **PI**–**PVI** and the unpublished MERIS investigations (**UP**). It is organised according to the three main themes of the thesis: optical modelling, interpretation algorithms and comparison of spatial and discrete water quality information. Discussion includes comparison of the results with the published results of other investigators and implications of the results for the application of remote sensing in lake monitoring.

3.1 Bio-Optical modelling

3.1.1 Absorption, scattering and reflectance models

The total absorption and scattering coefficients, needed in the R, K_d and Z_{SD} models, were obtained from CPS concentrations and SIOPs (**PI**). The variation in some SIOPs in lakes can be large (Strömbeck 2001, Herlevi 2002), but the optical data available did not allow the estimation of the regional or temporal SIOP variation. Therefore, average SIOPs were used in all optical models.

The SIOPs (Table 4) were mostly in line with published values for lakes. The S_{CDOM} was within the range that has been reported for lakes in Estonia and Finland (mean value: 0.015–0.017 nm^{-1}) (Sipelgas et al. 2003) and Sweden (mean value 0.015 nm^{-1}) (Pierson & Strömbeck 2001). The S_{tri} was in agreement with the mean values (0.010–0.013 nm^{-1}) from several other lake studies (Strömbeck 2001, Reinart et al. 2004, Dall'Olmo & Gitelson 2006, Binding et al. 2008). The $a^*_{\underline{TSS}}(400)$ was close to that measured in lakes in the USA (0.124 m^2 g^{-1}) by Dall'Olmo & Gitelson (2006b). Calculation of $a^*_{ph}(\lambda)$ as a function of $C_{Chl\text{-}a}$ is an improvement over many other lake models (e.g. Gege 2002, Dall'Olmo & Gitelson 2006a), where fixed $a^*_{ph}(\lambda)$ is assumed or $C_{Chl\text{-}a}$-dependency of ocean waters is used. This enables more realistic simulation of optical properties in lakes with considerable variation in $C_{Chl\text{-}a}$ than the fixed $a^*_{ph}(\lambda)$ approach does.

Table 4. SIOPs used in the optical models.

Coefficient	Symbol	Value	Source
Absorption coefficient of pure water	$a_w(\lambda)$	see the reference	Buiteveld (1994)
Specific absorption of phytoplankton	$a^*_{ph}(\lambda)$	see text	Ylöstalo (unpublished)
Spectral slope coefficient of CDOM absorption	S_{CDOM}	0.0150 nm^{-1}	PI
Specific absorption of bleached TSS at 400 nm	$a^*_{\underline{TSS}}(400)$	0.13 m^2 g^{-1}	Ylöstalo (unpublished)
Spectral slope coefficient of tripton absorption	S_{tri}	0.012 nm^{-1}	Ylöstalo (unpublished)
Specific scattering of TSS at 555 nm	$b^*_{TSS}(555)$	0.811 m^2 g^{-1}	PI
Scattering exponent of TSS	n_b	0.705	PI
Scattering coefficient of pure water	$b_w(\lambda)$	see the reference	Buiteveld (1994)
Backscattering ratio of pure water	$\hat{b}_{bw}$	0.5	Sathyendranath *et al.* (1989)
Backscattering ratio of TSS	$\hat{b}_{b,TSS}$	0.0131	PI

The backscattering ratio of TSS (Table 4) was slightly lower than in Dutch lakes (0.0157, Dekker 1993). The $b^*_{b,TSS}(555)$ of 0.0106 m^2 g^{-1}, calculated from the backscattering ratio and the scattering coefficient presented in Table 4, was in agreement with other lake studies. In the Dutch Lake IJsselmeer, for example, the $b^*_{b,TSS}(550)$ was 0.011 m^2 g^{-1} (Hoogenboom et al. 1998a). Heege and Fischer (2004), assuming wavelength-independent backscattering, reported a somewhat lower $b^*_{b,TSS}$ of 0.0086 m^2 g^{-1} for Lake Constance.

Scattering was simulated here without consideration for particle type. Optical modelling could be improved by considering inorganic particles and phytoplankton separately with characteristic scattering properties. For example, waters dominated by inorganic particles have backscattering ratios of a few per cent (Boss et al. 2003), while the phytoplankton-dominated ocean waters have lower backscattering ratios, such as 0.5% (Sathyendranath et al. 1989) and 1% (Oishi et al. 2002). Also in lakes the backscattering ratio has been reported to be higher for inorganic particles than for phytoplankton (Strömbeck 2001, Reinart et al. 2004).

Comparison of SIOPs published by different researchers is sometimes difficult because of the variety of methods applied. For example, the estimation of S_{CDOM} from measured $a_{CDOM}(\lambda)$ is not standardised and the method of $a_{CDOM}(\lambda)$ measurement applied by different researchers differs by filter type and pore size used in the filtering of water samples and in the correction of spectrophotometric measurements for residual scattering and baseline shift (e.g. Aas 2000, Sipelgas et al. 2003, Twardowski et al. 2004). Many of the optical methods for water remote sensing have been developed specifically for the ocean waters (NASA 2003). Validation measurements for lakes have been compiled e.g. by Pierson et al. (1999) and Kallio et al. (2007).

The measured R in the optical dataset (**PI**) showed considerable variation in its maximum values (0.01–0.08) and in the shape of the spectra among the lakes (Figure 4). The level of the modelled

reflectance and the shape of the spectra were generally in good agreement with measured values (Figure 4). The noise in the 400–450 nm region of the measured R at some stations is due to the low E_u, which is close to the lower measurement limit of the LI-1800UW spectrometer. The greatest discrepancies between the simulated and measured reflectances were in the eutrophic lakes (in the top row in Figure 4). The SIOPs can vary by lake (e.g. Strömbeck & Pierson 2001) and in eutrophic lakes the absorption and backscattering properties of phytoplankton have a strong impact on the reflectance.

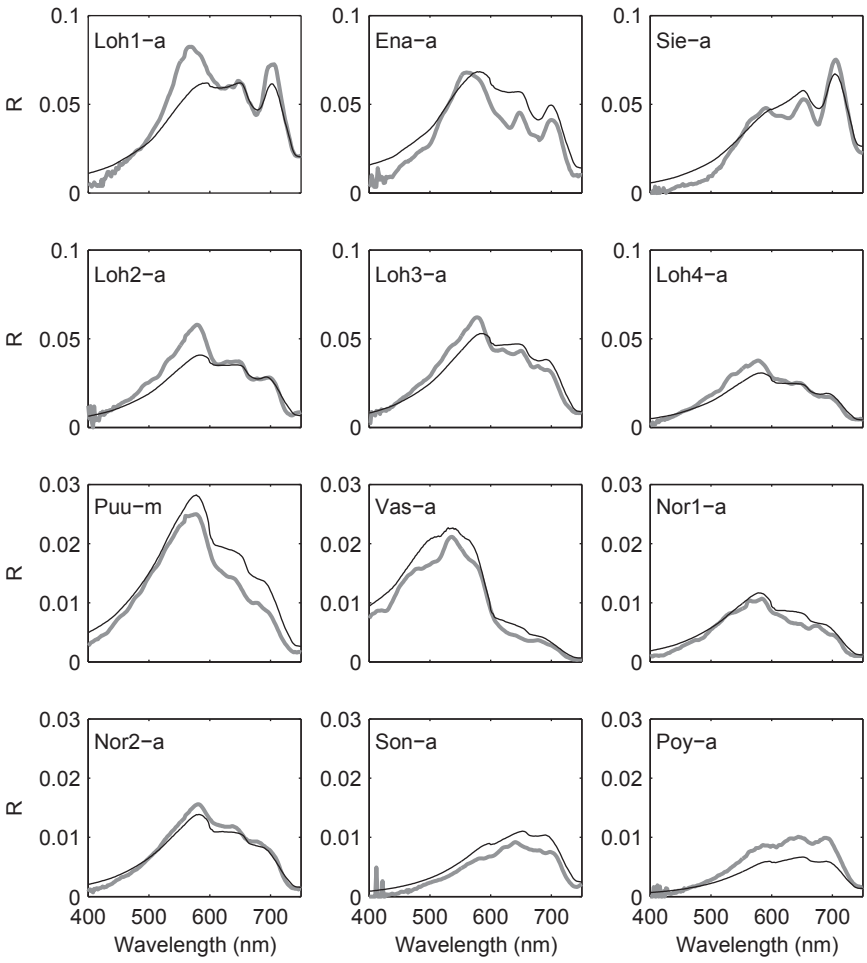

Figure 4. Measured (▬) and simulated (—) $R(\lambda)$ of the optical stations (**PI**). R^2 = 0.92 and RRMSE = 25% (for simulated vs. measured R in the 400-750 nm range of all 12 stations). Note the two scales on the y-axis. Simulated $R(\lambda)$ was calculated via Equations 12 and 22. SIOPs needed in the calculation of a_{tot} and $b_{b,tot}$ are presented in Table 4. The CPS concentrations and selected optical properties of the stations are presented in the appendix.

3.1.2 K_d and Z_{SD} models

Kirk's K_d model (Equation 24) with fixed coefficients g_1 and g_2 produced as good estimations as the K_d model (Equation 25) with calibrated coefficients (Figure 5). Kirk's model has been applied to Finnish lakes before, with measured a_{tot} and b_{tot} at nine wavelengths as input to the model (Herlevi 2002). Herlevi tested several other simple $K_d(\lambda)$ models and found that the optimal empirical coefficients varied somewhat by lake type. Strömbeck (2001) also used Kirk's model in the estimation of K_d(PAR) in Swedish lakes from CPS concentrations and average SIOPs, but spectral comparisons were not made.

Calibration of the two Z_{SD} models resulted in $Z_{SD} = 11.4/(c_{tot}(\text{PAR})+K_d(\text{PAR}))$ and $Z_{SD} = 7.26/c_{tot}(\text{PAR})$ (**PII**). The statistical accuracy characteristics of the two models were almost the same, with R^2 about 0.96 and RRMSE about 19% (N=14). The empirical coefficient C_2 of the first model was somewhat higher than those obtained by other investigators; for example, Tyler (1968) reported $C_2 = 8.69$ (Z_{SD} range: 10–48 m) and Holmes (1970) $C_2 = 9.42$ (2–12 m). Davies-Colley (1988) found $C_2 = 9.52$ (0.42–17.7 m) for lakes in New Zealand.

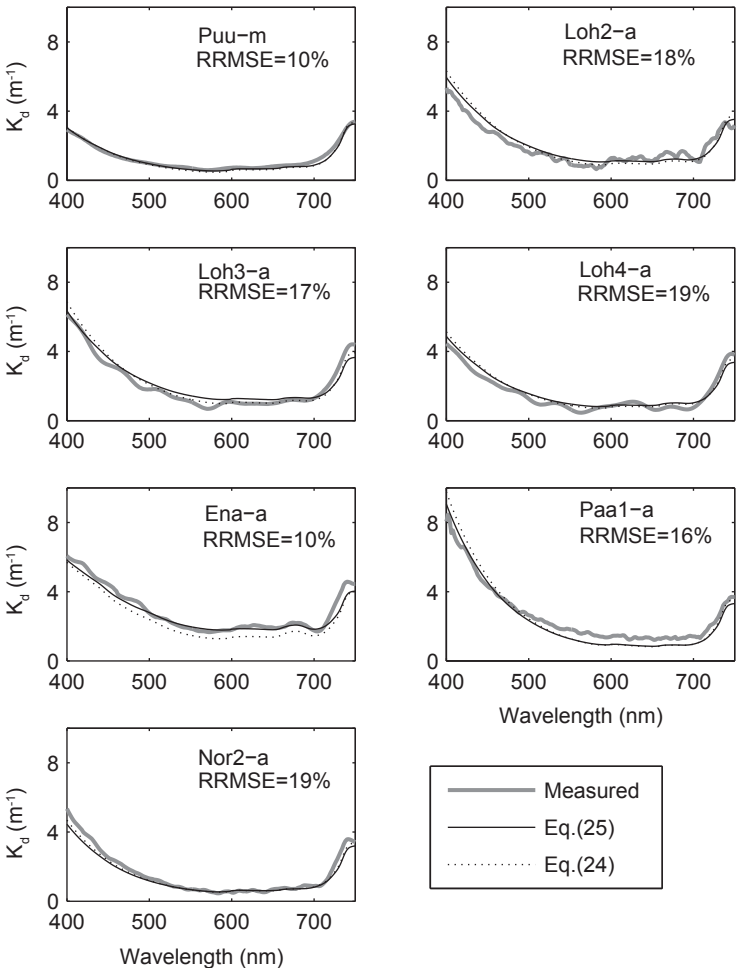

Figure 5. Simulated $K_d(\lambda)$ according to Equation (24) and Equation (25), and measured $K_d(\lambda)$ (redrawn from **PII**) in the optical stations. RRMSE is presented for $K_d(\lambda)$ simulated by means of Equation 25.

The optical models gave reasonable results in lakes with large differences in CPS concentrations and in different geographical regions. The optical models presented here are semi-empirical and do not take into account in detail, for example, the factors related to measurement geometry. Advanced optical modelling requires models such as Hydrolight (Mobley 1994, Mobley & Sundman 2007), which is utilised in the MERIS Boreal Lakes processor (Doerffer & Schiller 2008a, **UP**). The SIOPs may in reality differ from those assumed in the models, but the presented models are useful as general tools for various applications. The reflectance model is a module for inversion-based interpretation algorithms (**PI**) and for estimation of the influence of CPS and SIOP variation on semi-empirical algorithms (**PII** and **PVI**). The results obtained here indicated that $K_d(\lambda)$ can be calculated with Kirk's model (Equation 24) from measured CPSs and average SIOPs with reasonable accuracy in lakes with large CPS variations. The $K_d(\lambda)$ and Z_{SD} models presented are also ready modules for remote sensing algorithms (e.g. Kallio et al. 2009).

3.2 Interpretation of CPSs and Z_{SD}

The semi-empirical algorithms were investigated by means of optical (**PI**) and remote sensing data (**PIII**–**PVI**; see Figure 1). The AISA campaigns provided a large dataset with varying lake types and enabled investigation of lake-type-specific algorithms. Applicability of the semi-empirical algorithms was additionally studied through the simulations of $R(\lambda)$ using the CPS data from the national dataset, with particular focus on the influence of CDOM on interpretation. The results of the inversion algorithm applied to the optical station data are discussed in the satellite channel configuration section.

3.2.1 Semi-empirical algorithms

Previous studies have shown that in lakes with trophic status ranging from mesotrophic to hypereutrophic *Chl-a* is best estimate by the NIR-red ratio algorithm (e.g. Millie et al. 1992, Gitelson et al. 1993, Pierson & Strömbeck 2001). This was also the case with the airborne (**PIII**) and optical datasets (**PI**), where the highest correlation for $C_{Chl\text{-}a}$ was found with a radiance/reflectance ratio whose numerator is in the 685–715 nm and denominator in the 660–677 nm range (Table 5).

The best wavelength region for C_{TSS} and turbidity estimation was between 700–730 nm (Table 5, **PI** and **PIII**). According to the AISA data turbidity can be estimated with better accuracy than can C_{TSS}. The nephelometric determination of turbidity, which is based on an optical measurement, is an indirect approximation of scattering by particles, which directly influence reflectance. Another reason is that the measurement uncertainty of turbidity determination in the laboratory is less than that for C_{TSS} (**PIII**). The use of atmospherically corrected AISA data improved the estimation accuracy of the single-channel C_{TSS} and turbidity algorithms (**PIII**). This indicates that the atmospheric correction was able to smooth out the differences between campaign days to some extent.

According to the reflectance simulations using the national dataset (with fixed SIOPs, data from 1670 stations), $a_{CDOM}(400)$ was best predicted by linear regression against a ratio of reflectance at wavelength > 600 nm to reflectance in the 400–580 nm range (Fig. 6, **PII**). The simulation results were supported by the AISA (**PIII**) and LI-1800UW (**PI**) data. In this algorithm, the reflectance changes due to CDOM absorption in the short wavelength region are normalised by changes in reflection not related to CDOM in the longer wavelengths. The result is in accordance with the findings of Pierson et al. (2000) and Del Castillo & Miller (2008), among others, but here the algorithm was tested with a wider range of a_{CDOM} (with varying C_{TSS} and $C_{Chl\text{-}a}$) than in the investigations of other researchers.

Z_{SD} estimation via a channel ratio approach is site-specific, involving varying optimal channels and empirical coefficients (Härmä et al. 2001, Attila et al. 2008; **PII** and **PIII**). Z_{SD} measurement

Table 5. Summary of the channels and statistical accuracy characteristics of semi-empirical algorithms of AISA (**PIII**) and LI-1800UW (**PI**) data; R_{surf} is reflectance corrected for atmospheric disturbance according to de Haan and Kokke (1996). N is the number of measurements. The range column indicates the minimum and maximum values of measured *in situ* water quality and Z_{SD}.

Variable	Instrument	Channel or channel ratio	Month(s)	R^2	RMSE	RRMSE %	*N*	Range
$C_{Chl\text{-}a}$ µg l^{-1}	AISA	$L_u(699–705)/L_u(670–677)$	August	0.91	6.03	29	88	1.3–100
	AISA	$L_u(699–714)/L_u(661–667)$ (MERIS channels)	August	0.91	5.85	28	88	1.3–100
	LI-1800UW	$R(700–710)/R(660–670)$	July–August	0.96		27	12	0.8–73
Turb, FNU	AISA	$R_{surf}(705–714)$ (MERIS channel)	August	0.93	1.90	23	105	0.4–26
C_{TSS} mg l^{-1}	AISA	$R_{surf}(705–714)$ (MERIS channel)	August	0.85	2.86	32	74	0.7–32
	LI-1800UW	$R(700\text{-}710)$	July–August	0.98		18	12	0.4–20
Z_{SD}, m	AISA	$(L_u(661–667) – L_u(747–755))/(L_u(699–705) – L_u(747–755))$	August	0.85	0.52	31	107	0.4–7.0
$a_{cdom}(400)$, m^{-1}	AISA	$(L_u(567–574) – L_u(603–610))/L_u(603–610)$	August	0.84	0.81	20	47	1.2–14
	AISA	$L_u(661–667)/L_u(552–560)$ (MERIS channels)	August	0.78	0.92	23	47	1.2–14
	LI-1800UW	$R(660–670)/R(485–495)$ (MERIS channels)	July–August	0.98		14	12	0.3–18

in the field is influenced by all CPSs (and by several other factors, such as the measurement conditions and the reflectance of the disk – see Preisendorffer 1986). A generally applicable algorithm for the estimation of Z_{SD} and $K_d(\lambda)$ from remote sensing data that would not be sensitive to the independent variation of CPSs could be obtained by application of semi-analytical models (e.g. Equations 26 and 24) using $a_{tot}(\lambda)$ and $b_{tot}(\lambda)$ estimated from remote sensing data.

3.2.2 Limitations and improvements of the semi-empirical algorithms

The performance of the NIR-red *Chl-a* algorithm depends on the variation of $a^*_{ph}(\lambda)$, the specific backscattering coefficient of phytoplankton and other particles, S_{CDOM}, fluorescence and the concentration of inorganic particles and CDOM, as has been demonstrated in bio-optical simulation studies (Pierson & Strömbeck 2000, Strömbeck & Pierson 2001, Dall'Olmo & Gitelson 2005, Dall'Olmo & Gitelson 2006a). The key assumptions of the NIR-red ratio algorithm are: $a_{ph} >> bb_{TSS}$ and $a_{ph} >> (a_{CDOM}+a_{tri})$ in the 660–675 nm region (Gitelson et al. 2008).

In Lake Tuusulanjärvi, the empirical parameters of the *Chl-a* algorithm differed from those of the other eutrophic lakes in August (**PIII**). The accuracy of the *Chl-a* algorithm trained only for this lake was also lower than it was for the rest of the lakes. The fact that the ratio between turbidity and the $C_{Chl\text{-}a}$ was higher (0.42) than in the other four eutrophic lakes (0.21–0.29) of the AISA dataset indicates that the first key assumption of the NIR-red ratio algorithm, $a_{ph} >> bb_{TSS}$, was probably not fulfilled. The exceptional ratio between turbidity and the $C_{Chl\text{-}a}$ might be due to, for example, high concentration of inorganic particles.

The largest relative errors of NIR-red ratio algorithm with fixed wavelengths has been found for $C_{Chl\text{-}a} < 10$ µg l^{-1} (Gons et al. 2002, Dall'Olmo & Gitelson 2005). At low $C_{Chl\text{-}a}$, the NIR-red ratio becomes increasingly sensitive to the influence of other factors, especially to the variation of ($a_{CDOM} + a_{tri}$) and b_b (Dall'Olmo & Gitelson 2006a, Gitelson et al. 2008). The same NIR-red ratio cannot be optimal for a wide range of $C_{Chl\text{-}a}$, because the position of maximal radiance in the 685–715

nm region shifts to shorter wavelengths with decreasing $C_{Chl\text{-}a}$ (Gitelson 1992, Hoogenboom et al. 1998a). The use of a shorter wavelength in the numerator of the NIR-red ratio improved the estimation accuracy of $C_{Chl\text{-}a}$ in oligo- and mesotrophic lakes ($C_{Chl\text{-}a}$ < 25 µg l^{-1}) in the AISA data (**PIII**): the R^2 increased from 0.67 (for L(699–705)/L(670–677)) to 0.83 (for L(685–691)/L(670–677)). For oligotrophic lakes ($C_{Chl\text{-}a}$ < 10 µg l^{-1}) alone, the latter channel ratio yielded also reasonable accuracy (R^2 = 0.76, RRMSE = 27%, N = 30).

The second key assumptions of the NIR-red ratio algorithm, $a_{ph} >> (a_{CDOM}+a_{tri})$ in the 660–675 nm region (Gitelson et al. 2008), is critical for $C_{Chl\text{-}a}$ estimation in humic lakes. This was also proved by the AISA dataset, wherein the most humic lake, Keravanjärvi ($a_{CDOM}(400)$ = 14.3 m^{-1}, C_{TSS} = 4.4 mg l^{-1}, $C_{Chl\text{-}a}$ = 8.8 µg l^{-1}), was an outlier in the *Chl-a* estimation (**PIII**). Although a_{CDOM} in the 660–680 nm region is small in comparison to shorter wavelengths, it disturbs the $C_{Chl\text{-}a}$ algorithm by decreasing R in the 660–680 nm region, if CDOM concentration is high. This leads to higher NIR-red ratios and overestimation of $C_{Chl\text{-}a}$ if an algorithm calibrated for low CDOM is applied. The impact of a_{CDOM} on the NIR-red-ratio-based *Chl-a* algorithm has been earlier demonstrated in three Swedish lakes (Pierson & Strömbeck 2000, Strömbeck &Pierson 2001). The reflectance simulations with realistic CPS variations (national dataset; **PII**) showed that the accuracy of the NIR-red *Chl-a* algorithm is lowest in the lakes with high CDOM in all trophic classes (see Figure 6 for the mesotrophic lakes).

Accurate measurement and mathematical formulation of $a_{CDOM}(\lambda)$ in the 660–680 nm region are important for understanding of the limitations and development of lake-type-specific version of the NIR-red ratio algorithm, particularly in lakes with high CDOM. This was indicated through the sensitivity study of S_{CDOM} (**PII**). The use of a higher S_{CDOM} value, of 0.017 nm^{-1}, by Kallio (1999) and Sipelgas et al. (2003) instead of 0.015 nm^{-1} in the channel ratio simulation for the national dataset increased R^2 more in the high-CDOM lakes than in the low-CDOM lakes in all trophic levels (**PII**). The influence of S_{CDOM} variation on Chl-*a* estimation was strongest in the oligotrophic lakes with high CDOM: R^2 between $C_{Chl\text{-}a}$ and R(705)/R(675) increased in the high-CDOM subgroup of oligotrophic lakes from 0.76 to 0.88, when higher S_{CDOM} was assumed (**PII**). The C_{TSS} and $a_{CDOM}(400)$ algorithms were not sensitive to S_{CDOM}, as the changes in R^2 were negligible.

Some of the CDOM algorithms applied (Table 5) include a channel in the short-wavelength region, where high absorption combined with low particle concentration leads to low water leaving reflectance. Low light levels are difficult to measure accurately by remote sensing, because of the limitations in radiometric sensitivity. This may be one reason the CDOM estimation for the humic Lake Keravanjärvi ($a_{CDOM}(400)$ = 13 m^{-1}) was an outlier in the AISA dataset (**PIII**), although high CDOM was estimated satisfactorily in the humic lakes of the subsurface reflectance data (**PI**). The limitations of the semi-empirical CDOM algorithms are also discussed in section 3.2.4.

Remote sensing of a large group of lakes would benefit from the classification of lakes before interpretation. If hyperspectral data are available, the channels of *Chl-a* algorithms can be optimised by trophic status. In Finnish conditions, lakes should also be classified by their CDOM level (**PII** and **PIII**), which would enable separate training of, for example, the *Chl-a* algorithm by CDOM level and identification of lakes for which the accuracy of *Chl-a* estimation is expected to be lower than in other lakes. In the adaptive *Chl-a* algorithms (Ruddick et al. 2001, Dall'Olmo et al. 2003, Gitelson et al. 2008), optimal algorithms are selected directly according to the information included in the measured remote sensing data, but this approach requires hyperspectral data. Pulliainen et al. (2001) have shown that more comprehensive classification of lakes (by trophic status, and separation of humic and clear-water lakes) prior to the CPS interpretation can be performed from the shape of the radiance spectra of airborne spectrometer data.

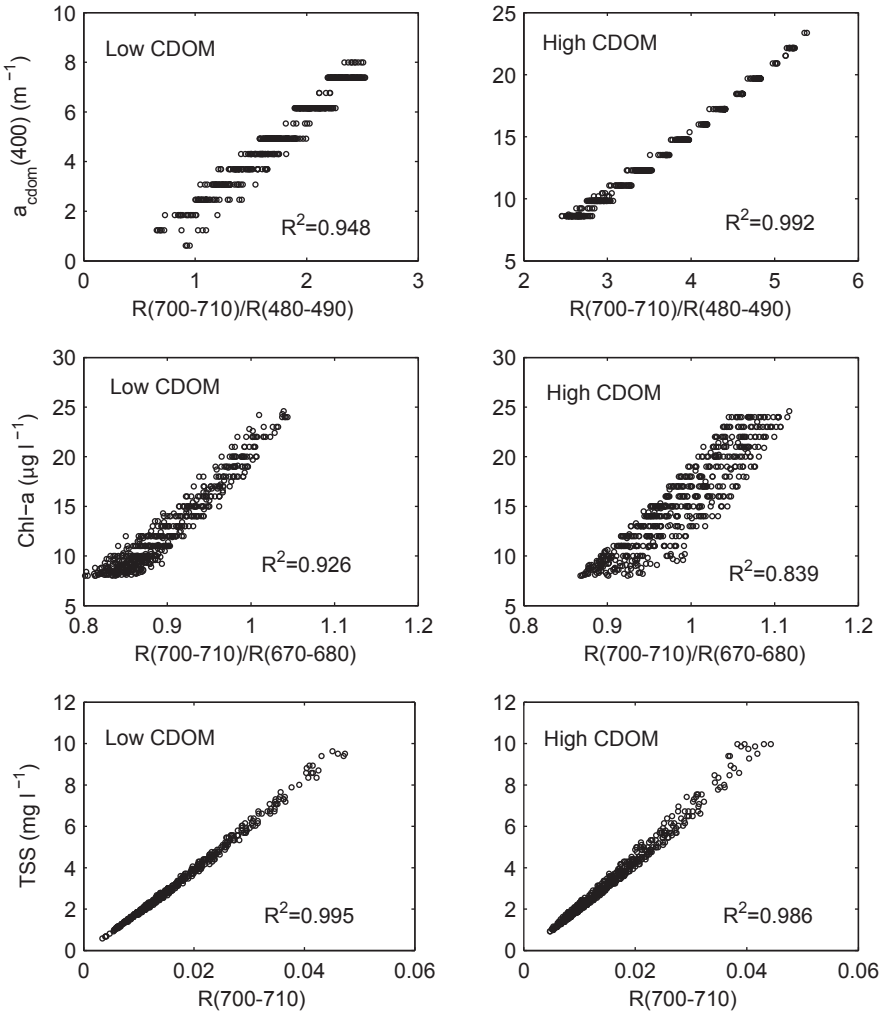

Figure 6. Relations between simulated channel ratios and measured CPSs in the low- (left column, $a_{CDOM}(400)$ < 8.61 m^{-1}, N = 547) and high- (right column, $a_{CDOM}(400) \geq$ 8.61 m^{-1}, N = 608) CDOM sub-groups in the mesotrophic lakes of the national dataset (**PII**).

3.2.3 Applicability of satellite instruments' channel configurations for CPS estimation

Knowledge of the suitability of the channel wavelengths of different satellite instruments for the estimation of CPSs is useful in, for instance, the selection of satellite imagery for a region of interest. The channel configurations of MERIS, MODIS and ETM+ were here investigated through the use of channels reconstructed from the measured hyperspectral R data (**PI**). MERIS and MODIS were included here because they were designed for water applications and provide images daily. ETM+ represents a large group of instruments first designed for land applications, but the data they provide would be valuable for lake monitoring, given their good spatial resolution. ETM+ has three wide channels, while MERIS and MODIS have several narrow ones in VIS and NIR (Table 3).

According to the airborne spectrometer study by Härmä et al. (2001), MERIS has the best channel configuration of the three satellite instruments for C_{TSS} and $C_{Chl\text{-}a}$ estimation in lakes and

coastal waters with semi-empirical algorithms. This result was confirmed here for C_{TSS} (based on R(700–710)) and $C_{Chl\text{-}a}$ (R(700–710)/R(660–670)) with measured $R(\lambda)$ data (**PI**). The essential difference between MERIS and MODIS is the 705 nm channel included in MERIS, which improves the accuracy of the estimation of C_{TSS} and $C_{Chl\text{-}a}$, particularly when the semi-empirical algorithms are used. The wide channels of ETM+ make the interpretation sensitive to the independent variation in CPSs (**PI, PVI**). However, the estimation of $a_{CDOM}(400)$, not included in the study of Härmä et al. (2001), was not sensitive to the width of the channels, as it was estimated with TM3/TM2 with the same accuracy as in the case of the narrow channels of MERIS (R(660–670)/R(485–495)) and MODIS (R(662–672)/R(483–493)) (**PI**).

The differences between instruments in the interpretation of CPSs by inversion (Figure 7) were similar to those of the semi-empirical algorithms applied to the same dataset (**PI**). Estimation of CPSs by inversion is sensitive to the variation of SIOPs (e.g. Gege 2002) and the estimation accuracy could be improved if information on lake-specific SIOPs were available. Based on the measured R data, MERIS has optimal or nearly optimal channels for CPS estimation by inversion (when compared with the use of continuous spectra 450–750 nm, 2 nm step) and semi-empirical algorithms (compared with the best channel or channel ratio in 450–750 nm, step 10 nm) (**PI**).

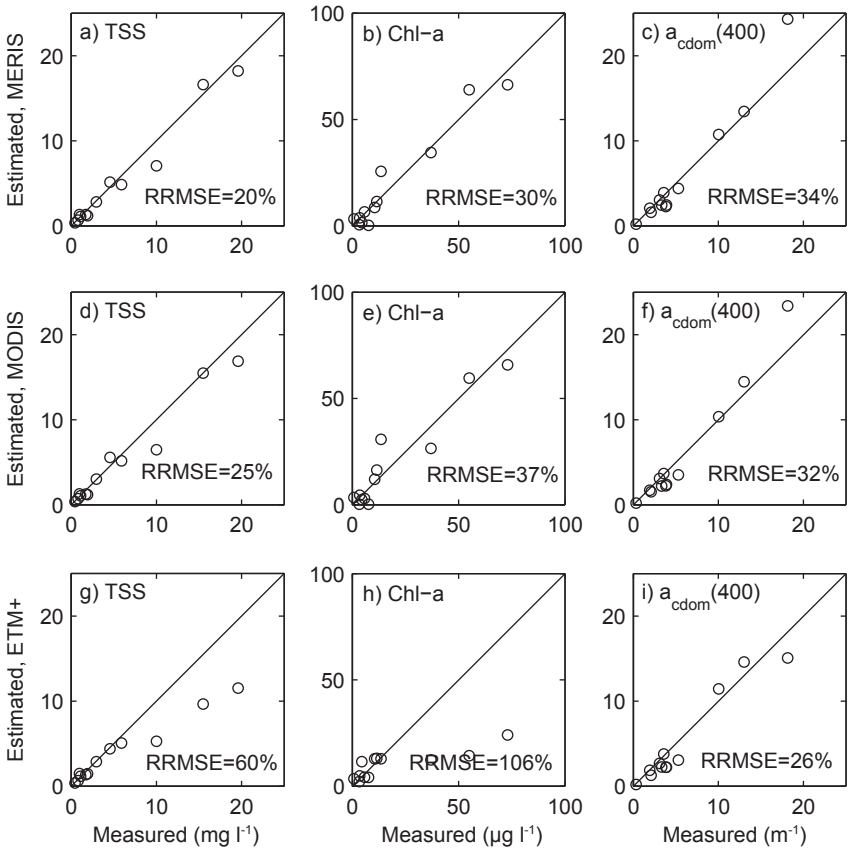

Figure 7. Relations between measured CPSs and CPSs estimated by the inversion of R (measured with LI-1800UW) using MERIS channels 2–10 (a–c), MODIS channels 2–8 (d–f) and ETM+ channels 1–3 (g–i) (**PI**).The inversion method is described in section 2.4.2 of the thesis.

3.2.4 ETM+ and ALI data

In addition to the channel position and width of a satellite instrument, interpretation accuracy for satellite measurements depends on the atmospheric disturbance and its correction, the measurement geometry, the radiometric characteristics of the instrument etc. The number of small lakes in boreal region (e.g. Raatikainen & Kuusisto 1988) can be high, with the monitoring by satellite remote sensing requiring sufficient spatial resolution. Water quality of small lakes can be mapped with TM-type instruments, but their limitations must be taken into account.

The average RRMSE of image-specific ETM+ algorithms trained with *in situ* data for turbidity, $a_{CDOM}(400)$ and Z_{SD} ranged from 17% to 23% (**PVI**). The relation between turbidity and TM3 was linear in May and July but was exponential in September (Figure 8). This is probably due

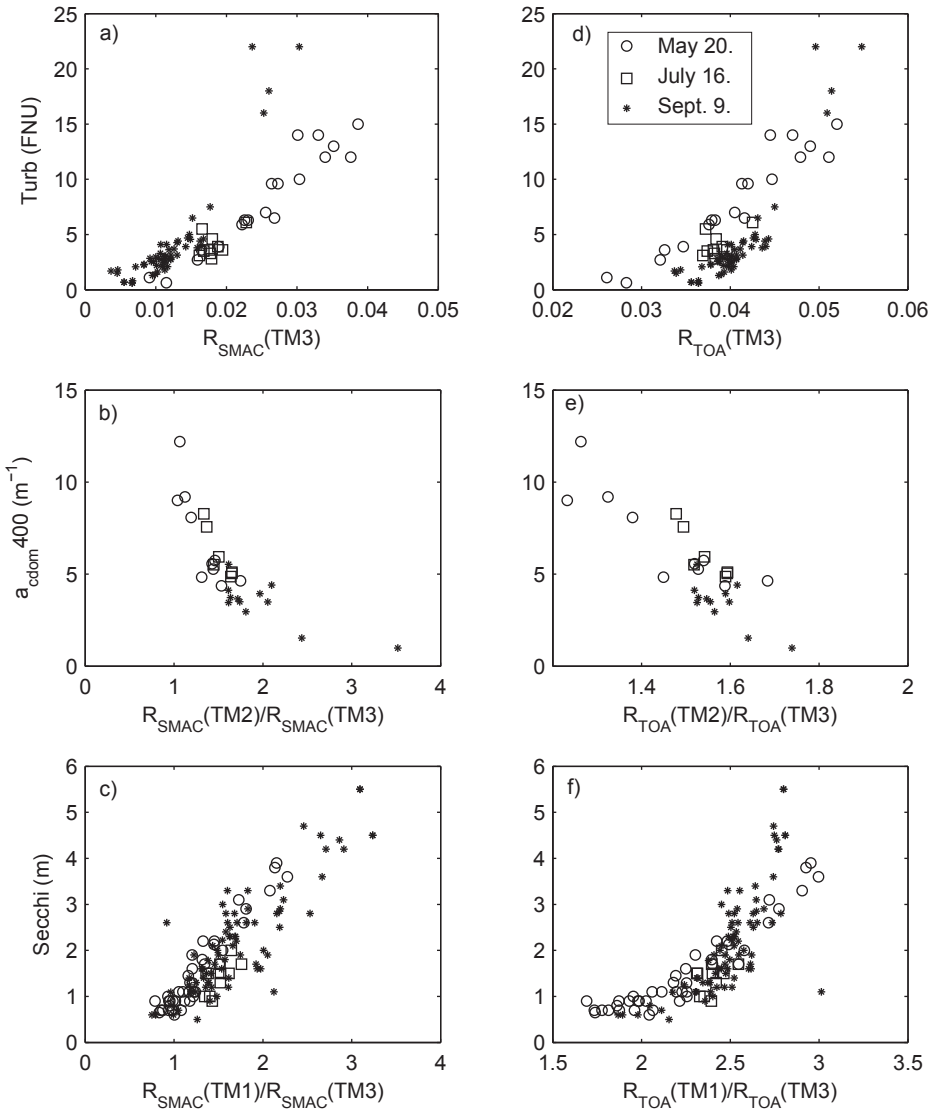

Figure 8. Relations between measured water quality variables (*Turb*, $a_{CDOM}(400)$ and Z_{SD}) and ETM+ reflectance and reflectance ratios (**PVI**). The left column (a–c) is for the SMAC-corrected reflectances and the right column (d–f) for TOA reflectances. Algorithm coefficients and statistical accuracy characteristics are shown in Table 6.

to the differences in the relative share of phytoplankton and inorganic particles, and the effect of phytoplankton absorption on reflectance at TM3. The variability of the relationship between turbidity and TM3 can also be seen in the *R* simulations using the national dataset (**PVI**) and with the semi-empirical algorithm for the measured *R* of the optical dataset (**PI**).

The Z_{SD} algorithm based on TM1 and TM3 has been used in several other studies of TM-type instruments (Lathrop 1992, Cox et al. 1998, Kloiber et al. 2002a, Brezonik et al. 2005). Z_{SD} is influenced by all three CPSs; therefore, a simple algorithm based on a channel ratio cannot be accurate if CPSs vary independently of each other (**PVI**). In some regions, conditions can be favourable for Z_{SD} estimation if, for example, turbidity and $C_{Chl\text{-}a}$ have a strong positive correlation with each another and strongly negative correlations with Z_{SD} (Brezonik et al. 2005). Here the estimation accuracy of Z_{SD} from ETM+ data was high in May (R^2 = 0.92) right after spring flooding, when $C_{Chl\text{-}a}$ was low and the correlation between turbidity and CDOM was high (**PVI**).

CDOM was estimated by ETM+ (**PVI**) and ALI (**PV**) with about the same accuracy. Differences in the performance of these two instruments could not be investigated here, because of the lack of simultaneous ETM+ and ALI data. According to the simulation study (**PV**), the 16-bit radiometric resolution of ALI enables estimation of a wider CDOM range with the TM2/TM3 ratio than the eight-bit radiometric resolution of ETM+ does.

High $a_{CDOM}(400)$ in combination with low backscattering leads to high absorption and consequently to low reflectance with the short wavelengths. Low water-leaving radiances are demanding to estimate by satellite instruments, because of atmospheric disturbances and possibly low radiometric sensitivity of the instrument. Doerffer (2008) estimated that the water-leaving radiance of the blue channels in waters with very high CDOM is near or even below the noise floor and calibration uncertainty of MERIS. Higher concentration of scattering particles increases water leaving radiance and decreases this problem. According to the results from the optical dataset and reflectance simulations (**PI** and **PII**), estimation of high $a_{CDOM}(400)$ is possible via semi-empirical algorithms in lakes with low turbidity if *R* (or R_{rs}) can be estimated with reasonable accuracy. Brezonik et al. (2005) reported that lakes with high CDOM ($a_{CDOM}(440)$ between 8 and 10 m^{-1}, corresponding to $a_{CDOM}(400)$ between 16 and 20 m^{-1}, if S_{CDOM} = 0.015 nm^{-1} is assumed) were outliers in Z_{SD} estimation by TM (based on the TM1 and TM3 channels). The ETM+ dataset included high CDOM values (up to $a_{CDOM}(400)$ of 12 m^{-1}), which were estimated with good accuracy. However, the high CDOM was connected to high turbidity (the correlation coefficient between $a_{CDOM}(400)$ and turbidity was +0.79).

Various atmospheric correction methods have been applied with TM-type instruments in lake applications (e.g. Dekker et al. 1992, Dekker et al. 2002, Hirtle & Rencz 2003, Vincent et al. 2004). However, the quantitative influence of atmospheric correction on the accuracy of estimation of water quality with TM-type instruments has seldom been reported. According to Klober et al. (2002a), atmospheric correction based on dark pixel subtraction and dark calibration targets applied to multi-temporal TM images were insufficient.

The SMAC atmospheric correction of the ETM+ data produced only a slight improvement in the overall estimation accuracy for $a_{CDOM}(400)$ and Z_{SD} as compared with the use of TOA reflectances (Figure 8 and Table 6). In the case of turbidity, the estimation accuracy was about the same for the various types of ETM+ data. However, the best turbidity algorithm for the TOA reflectances was based on the channel ratio, while the best algorithms for SMAC-corrected ETM+ data relied on a single channel. The channel ratios approximately compensate for differences in atmospheric disturbances by day and for the pixelwise variation in the atmosphere. They are also less susceptible to sun glint from waves than are the single-channel algorithms. The single-channel (TM3) turbidity algorithm was more accurate with SMAC-corrected reflectance (RRMSE = 29%; see Table 6) than with TOA reflectance (RRMSE = 53%), which indicates that the atmospheric correction balanced out the differences due to atmosphere disturbance to some extent over the three days.

Table 6. Interpretation algorithms and their statistical accuracy characteristics with SMAC-corrected reflectances and TOA reflectances – data from all three days were used in algorithm training. In the case of turbidity, two algorithms (linear and exponential) are shown for TOA reflectances (**PVI**).

Variable	Data	Algorithm	R^2	RMSE	RRMSE %	N	Range
Turb (FNU) [1]	SMAC	385.3*TM3 - 1.624	0.862	1.22	28.7	80	0.6–15
	TOA	570*TM3 - 18.4	0.535	2.25	52.6	80	0.6–15
	TOA	2389*exp(-2.72*TM1/TM3)	0.858	1.53	35.9	80	0.6–15
$a_{cdom}(400)$ (m^{-1})	SMAC	23.33*exp(-0.970*TM2/TM3)	0.830	1.18	22.3	29	1.0–12.2
	TOA	-18.1*(TM2/TM3)+32.9	0.721	1.28	24.3	29	1.0–12.2
Z_{SD} (m)	SMAC	1.806*(TM1/TM3) - 0.8903	0.778	0.52	26.9	131	0.5–5.5
	TOA	0.0299*exp(1.668*TM1/TM3)	0.729	0.67	34.5	131	0.5–5.5

[1]Four eutrophic/hypereutrophic lakes were not included in the calculation of turbidity statistics

The application of semi-empirical algorithms without image-specific training doubled the RRMSE on average (in worst case RRMSE for a single image was about 50% for $a_{CDOM}(400)$ and Z_{SD}) in comparison to the use of an image-specific algorithm (**PVI**). Accordingly, the method presented did not produce accurate enough CPS estimations without image-specific training and the application of ETM+ for water quality mapping (using the atmospheric correction procedure described here) with reasonable estimation accuracy requires simultaneous or near-simultaneous *in situ* measurements.

3.2.5 MERIS data

This section refers to the unpublished results of S. Koponen, K. Kallio and T. Pyhälahti (**UP**).

The previous validations of the MERIS lake processors were conducted with data from a few days – e.g. in Finland with data from three days (Koponen et al. 2008). The automatic measurement raft with observations at one-hour intervals in Lake Pyhäjärvi in 2009 made it possible to obtain validation data for every cloudless MERIS image, providing comprehensive data for algorithm testing in different atmospheric and lake conditions. The transect ac-9 measurements enabled the spatial test of the IOP (a_{tot} and b_{tot}) estimation by MERIS. This data was collected during the MERIS lakes project (Koponen et al. 2008), but the transect results shown here have not been published earlier.

The level of turbidity estimations generated by the Boreal Lakes processor was close to that of the automatic measurements (Figure 9). The *b(443)* produced by the processor was converted to turbidity with a conversion factor of 1.05 m FNU, which was based on the ac-9 measurements of 24 June 2009. For September, this conversion factor yielded too low turbidity. After the application of a higher conversion factor (1.72 m FNU) based on the ac-9 measurements of 16 September 2009, the correspondence between estimated and draft results in September was good (Figure 9). The correction (without bias) based on the comparison with raft measurements was small: $y = 1.11x$, where y = corrected value and x = value generated by the processor. The different scattering properties in September might be related to the occurrence of cyanobacteria, which were observed by the phycocyanin fluorometer installed on the measurement raft (Kallio et al. 2010).

According to the spatial comparison of IOPs in Lake Vesijärvi, Päijänne and Pyhäjärvi in 2007, the processor was able to estimate b_{tot} with RRMSE ≤ 16% (Figure 10). This confirms that turbidity and C_{TSS} can be estimated by the processor with reasonable accuracy, once the specific scattering coefficient is known.

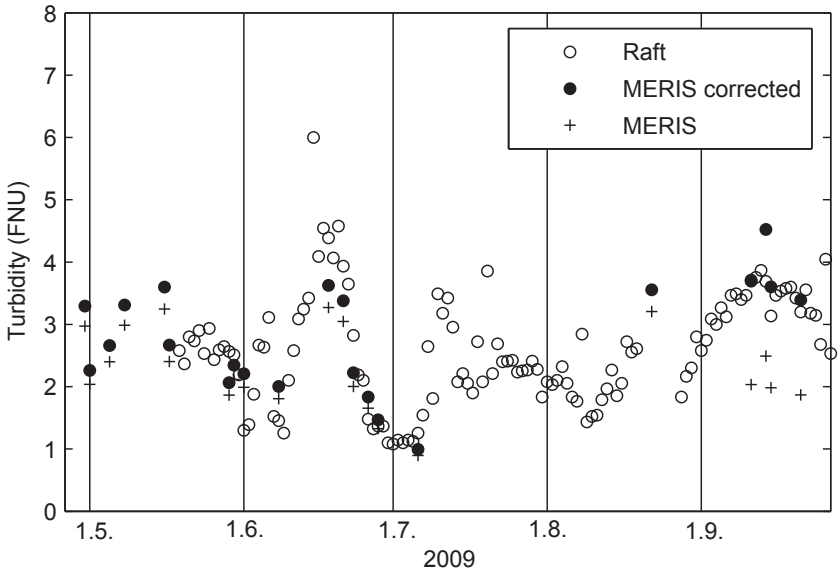

Figure 9. Time series of turbidity estimated from MERIS data by the Boreal Lakes processor (with ICOL pre-processing) and measured by automatic raft instruments in Lake Pyhäjärvi in 2009. MERIS = estimation generated by the processor, MERIS-corrected = processor estimation corrected by means of the raft data, raft = raft measurements. The accuracy characteristics of the corrected values were R^2 = 0.76 and RRMSE = 22%.

The $C_{Chl\text{-}a}$ estimated by the processor was overestimated by about 200% and $a_{CDOM}(443)$ was underestimated by about 40% in comparison to the raft (*Chl-a*) and interpolated (CDOM) measurements of Lake Pyhäjärvi in 2009 (detailed results are not shown), which is in line with the previous validation results of the processor (Koponen et al. 2008). After empirical correction R^2 was 0.36 (RRMSE=51%) for $C_{Chl\text{-}a}$ and 0.29 (RRMSE=36%) for $a_{CDOM}(443)$. The processor estimates followed the measured dynamics of both variables from May to September to some extent.

The discrepancies between the *in situ* measurements and semi-analytical interpretation of CPSs may be due to inaccuracies in SIOPs (*in situ* SIOPs differ from those assumed in the processor), R_{rs} (atmospheric and adjacency effect correction) or IOPs estimated by the processor. The spatial comparison in 2007 indicated that a_{tot} estimated by the processor corresponds well to the measured values or slightly underestimates them (Figure 11). In an experiment during the MERIS lake project, the processor estimated CDOM with reasonable accuracy with the bio-optical neural network of the Boreal Lakes processor, when $R_{rs}(\lambda)$ measured with a portable spectrometer was given as input (Koponen et al. 2008). While a^*_{ph} measurements were not available from 2009, previous validation measurements indicate that the overestimation of $C_{Chl\text{-}a}$ was not due to deviations in a_{ph}* (Kallio et al. 2009). The validation measurements from 2007 showed that the Boreal Lakes processor (with ICOL pre-processing) slightly overestimated R_{rs}, particularly in the blue region of the spectrum in oligotrophic lakes. These findings suggest that the problems in $C_{Chl\text{-}a}$ and CDOM estimation are related to the errors in the partition of a_{tot} between a_{ph} and a_{CDOM}, and in the atmospheric correction. Humic lakes with low backscattering level is an additional challenge to the Boreal Lakes processor, as was preliminary shown in the previous validation of the prosessor (atot(443) was clearly underestimated, Koponen et al. 2008).

The automatic raft and transect measurements increase the number of matches in validation of the satellite instruments considerably. In addition, temporally intensive *in situ* measurements enable studying the ability of an algorithm to estimate the seasonal dynamics of CPSs and they decrease the need for manual validation measurements during the satellite overflight.

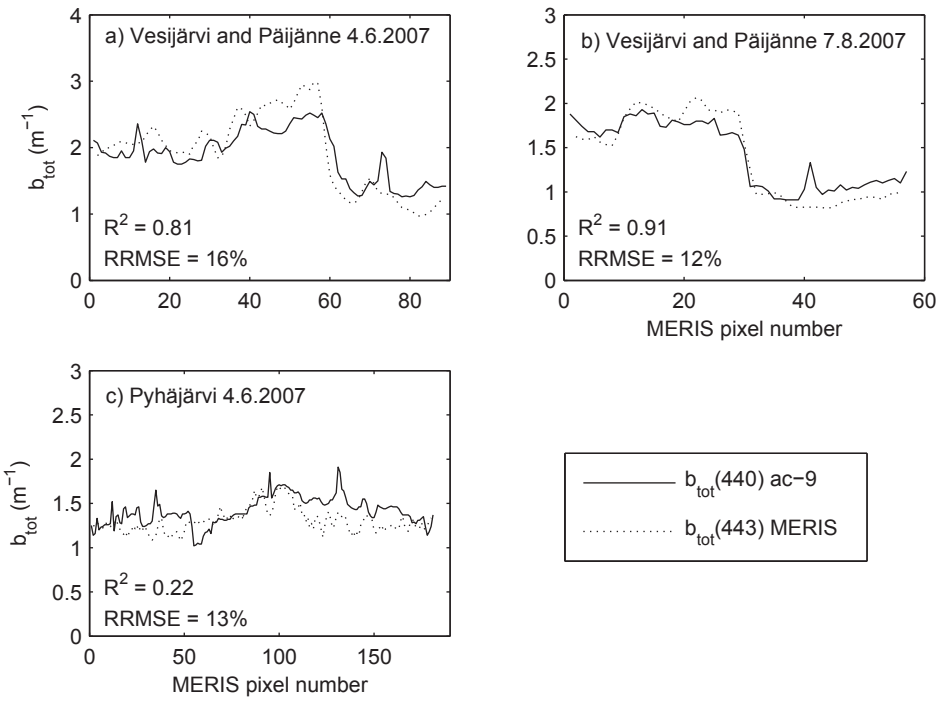

Figure 10. $b_{tot}(443)$ transects estimated from MERIS data by the Boreal Lakes processor (with ICOL pre-processing) and $b_{tot}(440)$ measured by ac-9. Panes a) and b) show the combined transects for Lake Vesijärvi and Päijänne for two days and pane c) shows the transect for Lake Pyhäjärvi. Lake Vesijärvi is represented in pane a) by pixel numbers 1-60 and in pane b) by pixel numbers 1-30. The rest of the pixels in panes a) and b) represent Lake Päijänne.

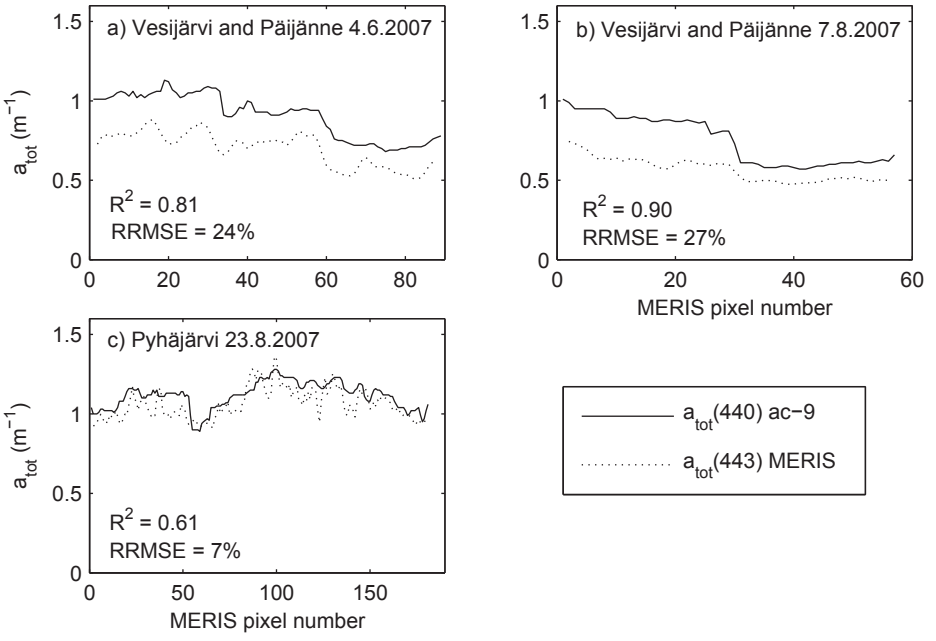

Figure 11. $a_{tot}(443)$ transects estimated from MERIS data by the Boreal Lakes processor (with ICOL pre-processing) and $a_{tot}(440)$ measured with ac-9. Panes a) and b) show the combined transects for Lake Vesijärvi and Päijänne for two days and pane c) shows the transect for Lake Pyhäjärvi. Lake Vesijärvi is represented in pane a) by pixel numbers 1-60 and in pane b) by pixel numbers 1-30. The rest of the pixels in panes a) and b) represent Lake Päijänne.

3.3 Comparison of spatial remote sensing data and discrete water quality information

Conventional monitoring provides numerically accurate information at one or a few locations in a lake and for selected lakes in a river basin, while remote sensing produces water quality information with good spatial resolution within a lake (**PIV, PVI**) and on different lakes over large areas (**PV** and **PVI**). The results of remote sensing mapping are usually reported in the form of concentration maps, but quantitative comparison with the information obtained by means of conventional sampling has seldom been carried out.

Airborne spectrometer data typically have high spatial resolution of a few metres and allow calculating estimates of overall water quality and its variation in a lake (**PIV**). At Lake Hiidenvesi, application of the lake-specific interpretation algorithm to AISA images revealed that $C_{Chl\text{-}a}$ can vary considerably even in short distances (Figure 12). The statistical characteristics of the discrete sampling stations were inadequate to describe the true spatial variation of $C_{Chl\text{-}a}$ (Table 7). The error for mean $C_{Chl\text{-}a}$ was large (about 50%) when the value calculated from the standard monitoring information (based on three routine monitoring stations) was compared with the AISA-based estimation. Remote sensing information can also be used to find representative locations of routine monitoring stations for the evaluation of changes in trophic status. In Lake Hiidenvesi, for example, the north-western part of the lake is oligotrophic and not part of the routine monitoring network.

Satellite instruments provide data for all lakes for which the image pixel size is sufficient. The 30 m resolution of the ETM+ images enables estimation of water quality in lakes of different sizes over large areas and of the spatial variation of water quality in large and medium-sized lakes. The spatial lake information derived from an ETM+ image shows the regional differences in water quality effectively (Figure 13). Because of the large number of lakes and the limited resources available for routine monitoring conducted via water sampling, monitoring can only cover some

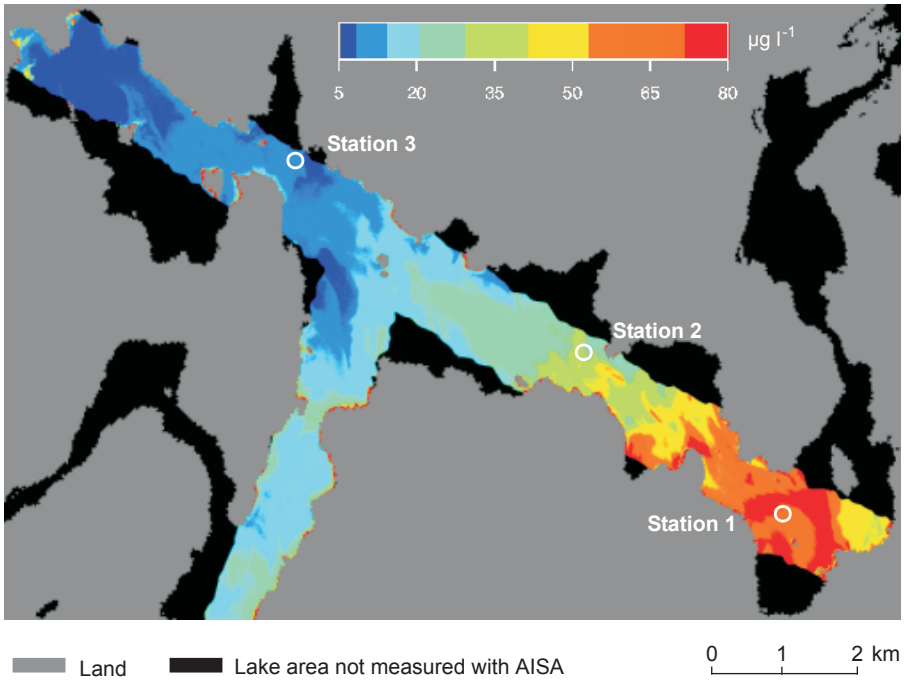

Figure 12. $C_{Chl\text{-}a}$ interpreted from AISA airborne spectrometer data for Lake Hiidenvesi on 11 August 1998. The locations of the three routine monitoring stations are indicated by white circles (redrawn from **PIV**).

Table 7. Standard errors and observed errors of estimated mean $C_{Chl\text{-}a}$ in Lake Hiidenvesi (modified from **PIV**). Observed error (difference to the AISA-based estimation) was calculated by Equation 35. The relative errors indicated in brackets were obtained by dividing the absolute errors by the true mean $C_{Chl\text{-}a}$, with the latter assumed to be the AISA-based estimation (25.2 µg l^{-1}) .

Dataset	Mean $C_{Chl\text{-}a}$ µg l^{-1}	Range of $C_{Chl\text{-}a}$, µg l^{-1}	Observed error µg l^{-1}	Standard error µg l^{-1}	Equation used for standard error
AISA data (*N*=3,010,748)	25.2	2.0–101	-	1.00 (4.0%)	(33)
Discrete stations (*N*=15)	22.4	6.2–70	2.78 (11.0%)	5.08 (20.2%)	(34)
Routine stations (*N*=3)	37.0	11–66	11.8 (46.9%)	15.9 (63.3%)	(34)

of the lakes. In the Siuntionjoki river basin, the use of ETM+-derived information enabled water quality estimation for 57 lakes (74% of all lakes ≥ 0.01 km2), while routine monitoring (water sampling) in 2000–2003 covered only 20 lakes (26%) (PVI). Fifteen lakes (19%) had enough water quality observations (at least three) for general usability classification of water bodies (Vuoristo 1998) based on the data from 2000–2003.

The use of TM-type instruments as an additional tool in water quality assessment would considerably increase the number of lakes for which at least some water quality estimates can be obtained. This makes possible more comprehensive comparison of lakes and river basins than the use of conventional monitoring data allows on its own. All lake information within an image is simultaneous, which is another advantage over routine monitoring, where only a few lakes can be sampled on any given day. Currently, the best interpretation technique for the TM-type images is to create image-specific algorithms using *in situ* data (**PVI**) either by means of specific field campaigns or through utilisation of near-simultaneous routine monitoring results.

The use of routine monitoring results for algorithm training requires that 1) the number of *in situ* observations be high enough and they represent different lake types, 2) the *in situ* observations provide information on CPSs and 3) observations represent the water layer that is measured by the remote sensing instrument. The routine monitoring results available vary greatly by image, but in some cases routine monitoring can provide sufficient data for algorithm training and validation. In the ETM+ study, the number of routine *in situ* observations (time window: ±3 days from satellite overflight) varied between eight and 20 in the area of the two river basins and in their vicinity (**PVI**). The combination of the number of *in situ* observations available and the width of the time window should be optimised for each image (e.g. Kloiber et al. 2002b). Knowledge of the seasonal differences in CPS variation (**PVI**) and the expected range of CPSs in conjunction with reflectance modelling (**PII** and **PVI**) can be utilised in algorithm selection and in identification of the algorithm's limitations. Routine monitoring in Finland normally provides information on the main CPSs: TSS (estimated on the basis of turbidity), *Chl-a*, CDOM (estimated from Pt colour) and Z_{SD}. In 2000, $a_{CDOM}(400)$ and C_{TSS} were added to the determinations in national monitoring programmes (mainly with intensively monitored stations) of the Environmental Administration in Finland for the needs of the development of remote sensing methods and optical applications. The routine monitoring samples are taken from a 1 m depth or as a composite sample from 0–2 m. The maximum z_{att} in Finnish lakes was between 0.45 and 2.20 m in 80% of the cases and the median value was 1.05 m (Table 4). Therefore, the routine monitoring results represent fairly well the surface layer measured by a remote sensing instrument.

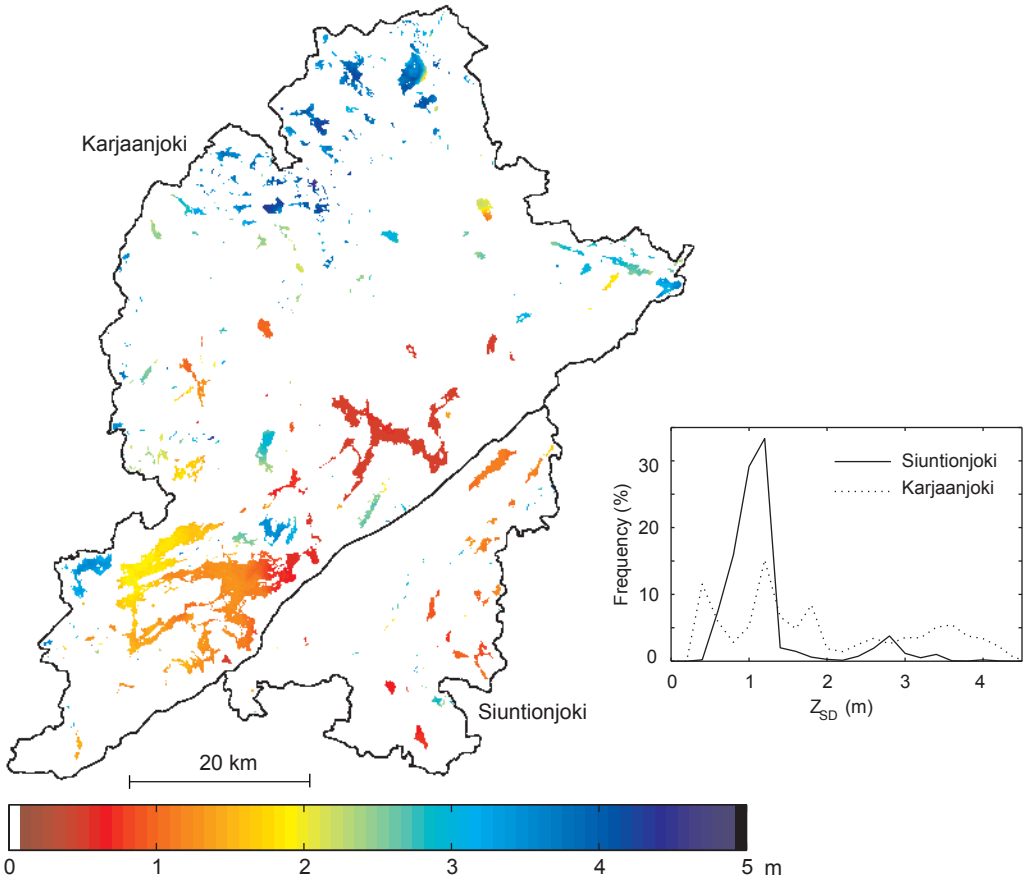

Figure 13. Z_{SD} in the Karjaanjoki and Siuntionjoki river basins as estimated from the ETM+ image on 20 May 2002 (**PVI**). The corresponding frequency distributions are presented in the small figure. The average Z_{SD}s were 1.2 and 1.9 m, respectively.

Conclusions and future perspectives

The main advantage of the use of remote sensing in lake-rich regions is that remote sensing yields water quality estimates for lakes not belonging to the routine monitoring networks, as demonstrated in the river basin studies of this thesis. Remote sensing also enables simultaneous comparison of the water quality of all lakes within an image. In lakes with a large spatial variation in water quality, the use of spatially high-resolution remote sensing data improves the accuracy of water quality estimation compared to conventional monitoring methods. The quantitative analyses of this study showed that routine monitoring results can yield as high as 50% under- or overestimation of the overall water quality of a lake. Remote sensing yields water quality information for the surface layer and for a limited number of variables primarily related to water transparency, trophic status and humic level, but when combined with conventional monitoring results, and with tools such as lake modelling, it aids in providing extensive information of lakes. Remote sensing has not yet reached a level that would enable its large-scale routine use in lake monitoring, mainly because of non-optimal satellite instruments and a lack of easily applicable interpretation algorithms. The methods presented here improve the interpretation of water quality from remote sensing data and

support its use in lake monitoring. The results are applicable also in other parts of the boreal region where the number of lakes is high and the CDOM varies considerably.

The optical models of this thesis were applied in a wide range of CPS combinations, including lakes with high CDOM. Combining the reflectance model and an extensive dataset of routine monitoring results helped to identify the limitations of the semi-empirical algorithms and the need for lake-type-specific algorithms; obtaining a similar amount of reflectance spectra via radiometric measurements in the field is very laborious. The strength of this approach is the fact that the algorithm simulations represent realistic combinations of CPSs in the region of interest.

Knowledge about optical properties and their modelling could be utilized in the monitoring and managing of lakes more than is currently done today. The finding that the $K_d(\lambda)$ can be estimated with reasonable accuracy from the measured CPS concentrations, for example, enables us to gain more detailed information on light attenuation from routine monitoring results than can be obtained via the routinely measured Z_{SD}. This detailed information on attenuation may be usable in ecological applications.

The optical models of this thesis relied on the average SIOPs determined for Finnish lakes, since the optical data did not allow us to take into account SIOPs for different seasons, lake types and regions. Such information would be useful for the further improvement of the optical models and remote sensing algorithms. More information is also needed on backscattering and the contribution of phytoplankton and inorganic particles to scattering. Because of the high impact of CDOM on absorption and reflectance in many Finnish lakes, the $a_{CDOM}(\lambda)$ should be known and modelled with good accuracy throughout the visible region. Alternative methods for $a_{CDOM}(\lambda)$ determination not sensitive to the presence of small particles, such as the Point-Source Integrating-Cavity Absorption Meter (PSICAM) (e.g. Röttgers & Doerffer 2007), should be tested.

The error from remote sensing-based estimates (AISA, ETM+) was mainly between 10 and 30% when simultaneous *in situ* measurements were used for algorithm training. The estimation accuracy of semi-empirical algorithms can be improved by classifying the lakes prior to interpretation and by creating lake-type-specific algorithms. This is particularly the case with $C_{Chl\text{-}a}$, which benefits from the pre-classification of lakes by their trophic status. This study indicated that in regions with a wide CDOM range, lakes should additionally be classified according to their CDOM level before $C_{Chl\text{-}a}$ interpretation.

The use of TM-type instruments in addition to routine monitoring results substantially increases the number of lakes for which water quality information can be obtained. The planned TM-type instruments will be better suited to remote sensing of water quality than what is currently available for operational use. Sentinel-2 MSI (http://www.esa.int/esaLP/SEMM4T4KXMF_LPgmes_0.html) and LDCM OLI (http://ldcm.nasa.gov/), both scheduled to be launched in 2012, will provide 12-bit data. In addition, the MSI will include a 30-nanometre-wide channel near the red absorption peak of phytoplankton and a 15 nm wide channel at 705 nm. This means an improved estimation accuracy for turbidity and C_{TSS} and may enable the estimation of $C_{Chl\text{-}a}$ with a good spatial resolution (10–20 m). Reflectance modelling and experimental hyperspectral data indicated that MERIS has optimal or nearly optimal channels for CPS estimation in Finnish lakes. Because of the 300 m spatial resolution, MERIS images are suitable only for large and medium-sized lakes. These lakes often belong to the routine monitoring network, but MERIS images can be utilised in producing CPS information for different parts of large lakes, and in filling in the gaps resulting from conventional monitoring. The limitations of satellite remote sensing in humic lakes with low backscattering levels should be studied with a more extensive dataset than that available in this study.

The preliminary results of this thesis indicated that CDOM can be estimated with TM-type satellite instruments. The future TM-type instruments will be more suitable for CDOM estimation, particularly in terms of their radiometric characteristics and the number of channels designed for atmospheric correction. Large-scale CDOM mapping with good spatial resolution could be used

as an aid in the global estimation of the role of lakes in global carbon budgets. The recent study of Griffin et al. (2011) showed that TM-type instruments can also be utilized in the assessment of carbon flux from large river systems to the sea.

Algorithms that would not require simultaneous *in situ* data for algorithm training would increase the amount of remote sensing-based information usable for lake monitoring. These algorithms should be based on the regional characteristics of SIOPs and the atmosphere, and on the typical variation of CPS. The analytical algorithm of the MERIS Boreal Lakes processor, trained with the optical properties and CPS ranges typical of Finnish lakes, enabled turbidity estimations with good accuracy without the need for image-specific algorithm correction with simultaneous *in situ* measurements. Using the processor to estimate *Chl-a* and CDOM with reasonable accuracy requires better partitioning of a_{tot} to a_{ph}, and a_{CDOM} and enhanced atmospheric correction. *Chl-a* estimation by the processor in boreal lakes could possibly be improved via better modelling of the red-NIR region, where the influence of CDOM on reflectance is small.

The development and validation of remote sensing algorithms is often based on manual sampling and measurements, which only provide occasional discrete data. The automatic raft and transect measurements used here yield, temporally and spatially, a high number of match-ups for the validation and development of algorithms in different conditions and thus aid in the creation of better remote sensing products. In addition, comprehensive measurement campaigns (SIOPs, R_{rs}, atmospheric parameters) similar to those of the MERIS Lake project would provide essential material for the testing and development of various processors.

Yhteenveto

Järvien seuranta perustuu nykyisin pääasiassa manuaaliseen näytteenottoon ja näytteiden analysointiin laboratoriossa. Runsasjärvisillä alueilla kuitenkin vain pientä osaa järvistä pystytään seuraamaan perinteisin menetelmin. Yksi mahdollisista menetelmistä parantaa seurannan alueellista kattavuutta on järvien kaukokartoitus lentokoneen tai satelliittien avulla.

Tämän työn tavoitteet olivat tutkia vedenlaadun tulkinta-algoritmeja suomalaisissa järvissä, kehittää optisia malleja tulkinnan avuksi ja valon tunkeutumisen arvioimiseksi sekä verrata kaukokartoituksella saatavaa tietoa perinteisten menetelmien tuottamaan tietoon. Tutkimuksen aineistot koostuivat optisista mittauksista, satelliitti- ja lentokonekuvista yhdessä samanaikaisten *in situ* havaintojen kanssa, automaattimittauksista ja järviseurannan tuloksista koko Suomesta.

Tarkan resoluution kaukokartoituskuvat osoittivat, että rehevissä järvissä perinteisen menetelmillä saatava arvio voi poiketa jopa 50 % järven todellisesta *a*-klorofylli pitoisuudesta. TM-tyyppisten satelliittikuvien (erotuskyky tyypillisesti 30 m) käyttö lisää huomattavasti niiden järvien määrää, joista saadaan vedenlaatuarvioita (pääasiassa sameudesta). Tulokset osoittivat myös alustavasti, että TM-tyyppiset instrumentit soveltuvat humuspitoisuuden arviointiin. Laajojen alueiden humuskartoituksia voitaisiin mahdollisesti hyödyntää arvioitaessa järvien vaikutusta hiilitaseisiin. MERIS satelliitti-instrumentin kanavat ovat optimaaliset tai lähes optimaaliset sameuden, kiintoaineen, *a*-klorofyllin ja humuksen arviointiin Suomen järvissä. MERIS kuvia (erotuskyky 300 m) voidaan käyttää suurten ja keskisuurten järvien eri osien tilan arvioinnissa sekä arvioitaessa niitä tämän kokoluokan järviä, jotka eivät kuulu seurantaohjelmiin. Menetelmät, jotka eivät vaadi *in situ* havaintoja algoritmien kalibrointiin, lisäisivät huomattavasti käyttökelpoisten kaukokartoitusarvioiden määrää. Tässä työssä osoitettiin, että analyyttinen MERIS Boreal prosessori, jonka opettamiseen käytettiin tämän tutkimuksen optisia ominaisuuksia ja vedenlaadun vaihteluvälejä, arvioi sameutta hyvällä tarkkuudella ilman kuvakohtaista kalibrointia. *a*-klorofylli ja humuksen arviointi MERIS Boreal prosessorilla kohtuudella tarkkuudella vaatii vielä kokonaisabsorptiokertoimen tarkempaa jakamista eri komponentteihin. Satelliittikaukokartoituksen soveltuvuutta humusjärvien vedenlaadun arviointiin tulisi tutkia laajemmalla aineistolla kuin mitä tässä työssä oli

käytettävissä. *a*-klorofyllin arviointitarkkuutta empiiristen kanasuhteiden avulla voidaan tarkentaa jakamalla järvet ryhmiin humus- ja rehevyystason mukaan.

Tässä työssä hyödynnettiin vedenlaadun automaattimittauksia ja optisten ominaisuuksien linjamittauksia. Nämä mittaukset mahdollistavat kaukokartoitusmenetelmien tehokkaan testauksen tuottamalla ajallisesti ja paikallisesti kattavaa vertailuaineistoa. Veden optiikan tietämystä voitaisiin hyödyntää nykyistä enemmän järvien seurannassa ja hoidossa. Tässä työssä osoitettiin, että valon vaimenemista eri aallonpituuksilla voidaan mallintaa luotettavasti rutiiniseurannan vedenlaatumittausten perusteella.

Tämän tutkimuksen tulokset parantavat vedenlaadun tulkintaa kaukokartoitusaineistoista ja tukevat kaukokartoituksen käyttöä järvien seurannassa.

Acknowledgements

Before I started work on the remote sensing, I was dealing with acidification problems, climate change, agricultural nutrient load modelling and lake modelling. I have always been interested in new techniques and methods that provide new perspectives on environmental problems. Work on remote sensing led me back to the basic limnology, this time with a strong emphasis on the fate of light. Through several field trips of this work, I was able to experience in practice the huge variety of lake types and environments in Finland.

I want to thank my supervisor, Jouni Pulliainen, for his valuable guidance and for commenting on the manuscript of the summary paper. I appreciate Jouni's ability to make successful funding applications and get people from different institutes work together. The thorough comments by the reviewers, Dmitri Pozdnyakov and Anssi Vähätalo, helped me improve the summary paper.

I am grateful to Lea Kauppi, director general of the Finnish Environment Institute (SYKE), for her positive attitude to this work. Lea also introduced me to research work in the beginning of my career. Juha Kämäri is acknowledged for providing me the opportunity to start working with remote sensing. I want to thank my bosses Matti Verta, Saara Bäck, Anna-Stiina Heiskanen, Juha-Markku Leppänen and Heikki Pitkänen for various types of support during the course of this work.

Close co-operation with the remote sensing specialists of SYKE, Jenni Attila (neé Vepsäläinen), Timo Pyhälahti, Pekka Härmä, Tuula Hannonen and Saku Anttila has been vital for this work. I want to thank Yrjö Sucksdorff for fostering cross-department co-operation in a remarkable way.

Collaboration with the Laboratory of Space technology (currently, the Department of Radio Science and Engineering, Aalto University) has been continuous during the course of this work. I particularly want to thank Martti Hallikainen and Simo Tauriainen. Sampsa Koponen, who just recently joined SYKE, is acknowledged for punctual and effective work in several joint projects. Kai Mäkisara and Karri Eloheimo had important roles in the realization of the AISA campaigns.

I am grateful to Pasi Ylöstalo and Jukka Seppälä for sharing their knowledge on absorption properties and for conducting absorption measurements. Matti Leppäranta and Antti Herlevi are acknowledged for co-operation in the optical field measurements. Tiit Kutser introduced me to bio-optical modelling and we have continued communicating on remote sensing ever since, regardless of Tiit's coordinates. I want to thank Ulla-Maija Hyytiäinen for her enthusiastic coordination of the Lohjanjärvi work package in the Karjaanjoki LIFE project; Ari Mäkelä is acknowledged for the idea of including satellite images in the same project.

Ahti Lepistö and Timo Huttula are acknowledged for successfully managing the multi-approach projects in Lake Pyhäjärvi, and Antti Lindfors and Mikko Kiirikki for several discussions on the automatic measurements. Arjen Raateland has provided programming help and Juhani Henttonen helped with several field campaigns. Maija Niemelä and Jokipii did phytoplankton countings. I want to thank Heidi Vuoristo and Sari Mitikka for the discussions on the needs of lake monitor-

ing and Pirkko Kortelainen for sharing her knowledge about humic lakes. Ritva Koskinen is acknowledged for doing the layout of the summary part and for reminding me about the schedule.

The Regional Environment Centres of Uusimaa, south-western Finland and Lapland provided important help in sampling and laboratory work. I am grateful to Helmi Kotilainen, Satu Vuolas, Markku Örn and Annukka Puro-Tahvanainen for their positive attitude towards the field campaigns.

The SALMON project was an important starting point for this work. I want particularly to thank Eugenio Zilioli (†), Tommy Lindell, Don Pierson and Niklas Strömbeck of the project team. The MERIS Lakes was a small but productive project; I want to thank Sampsa, Roland Doerffer, Antonio Ruiz-Verdú, Thomas Heege and Carsten Brockman for the stimulating atmosphere during the project.

Financial support from the Finnish Funding Agency for Technology and Innovation, the Academy of Finland, the European Space Agency, and the EU framework and LIFE programmes is gratefully acknowledged.

I want to thank Taina for her ability to make a joke of the small details of everyday life. I am thankful to my parents for supporting me in my endeavours and for introducing me to the aquatic environment since the very beginning. I also want to thank my brother, who has taught me several valuable skills such as cleaning a fish at the time when waters were still so transparent that perch were clearly visible under the clinker-built wooden hull.

References

Aas, E. 2000. Spectral slopes of yellow substance: problems caused by small particles. *Proceedings of the XV Ocean Optics Conference*, Monaco, 16-20 October, 2000. CD-ROM. 8 p.

Ahn, Y.H., Bricaud, A. & Morel, A. 1992. Light backscattering efficiency and related properties of some phytoplankters. *Deep-Sea Research 39*: 1835–1855.

Anttila, S., Pyhälahti, T., Vepsäläinen, J. & Kallio, K. 2005. *Rationalizing water quality monitoring by remote sensing and GIS – results of an end-user survey*. Internal report of Finnish Environment institute. 19 pp. (in Finnish with English summary).

Arst , H. 2003. *Optical Properties and Remote Sensing of Multicomponental Water Bodies*. Springer , Praxis Publishing , Chichester , UK. 238 pp.

Attila, J., Pyhälahti T., Hannonen T., Kallio K., Pulliainen J., Koponen S., Härmä P. & Eloheimo K. 2008. Analysis of Turbid Water Quality Using Airborne Spectrometer Data with a Numerical Weather Prediction Model-aided Atmospheric Correction. Photogramm. *Eng. Remote Sens.* 74: 363–374.

Binding, C. E., Greenberg, T. A., Jerome, J. H., Bukata, R. P. & Booty, W. G. 2011. An assessment of MERIS algal products during an intense bloom in Lake of the Woods. *J. Plankton Res.* 33: 793–806.

Binding, C.E., Jerome, J.H., Bukata, R.P. & Booty, W.G. 2008. Spectral absorption properties of dissolved and particulate matter in Lake Erie. *Remote Sens. Environ.* 112: 1702–1711.

Boss, E., Stramski, D., Bergmann, T., Pegau, W.S. & Lewis, M. 2004. Why should we measure the optical backscattering coefficient? *Oceanography* 17: 44–49.

Brezonik, P., Menken, K. D. & Bauer, M. 2005. Landsat based remote sensing of lake water quality characteristics, including chlorophyll and colored dissolved organic matter (CDOM), *Lake Reserv. Manage.* 21: 373–382.

Bricaud, A., Babin, M., Morel A. & Claustre, H. 1995. Variability in the chlorophyll-specific absorption coefficients of natural phytoplankton: Analysis and parametrization. *J. Geophys. Res.* 100 (C7): 13321–13332.

Bricaud, A., Morel, A. & Prieur, L. 1981. Absorption by dissolved organic matter of the sea (yellow substance) in the UV and visible domains. *Limnol. Oceanogr.* 26: 43–53.

Brivio, P.A., Giardino, C. & Zilioli, E. 2001. Determination of chlorophyll concentration changes in Lake Garda using an image-based radiative transfer code for Landsat TM images. *Int. J. Remote Sens.* 22: 487–502.

Buiteveld, H., Hakvoort, J.H.M. & Donze, M. 1994. The optical properties of pure water. Proceedings of the Ocean Optics XII Conference, *Soc. Photoopt. Inst. Eng.* 2258: 174–183.

Bukata, R.P. 2005. *Satellite Monitoring of Inland and Coastal Water Quality: Retrospection, Introspection, Future Directions.* CRC Press, Taylor & Francis. 246 p.

Bukata, R.P., Dekker, A.G. & Borstad, G.A., 2002. A clear view of turbid waters. *Backscatter* 13(1): 36–38.

Bukata, R.P., Jerome, J.H., Borstad, G.A., Brown, L.N. & Gower, J.F.R. 2004. Mitigating the impact of trans-spectral processes on multivariate retrieval of water quality parameters from case 2 waters. *Can. J. Remote Sensing* 30: 8–16.

Bukata, R.P., Jerome, J.H., Bruton, J.E. & Jain, S.C. 1979. Determination of inherent optical properties of Lake Ontario coastal waters. *Appl. Optics* 18: 3926–3933.

Bukata, R. P., Jerome, J. H., Kondratyev, K. Ya. & Pozdnyakov, D. V. 1991, Estimation of organic and inorganic matter in inland waters: optical cross sections of LakesLadoga and Ontario. *J. Great Lakes Res.* 17: 461–469.

Bukata, R.P., Jerome, J.H., Kondratyev, K.Y. & Pozdnyakov, D.V. 1995. *Optical Properties and Remote Sensing of Inland and Coastal Waters.* CRC Press, Boca Raton, FA. 371 p.

Carder, K.L., Steward, R.G., Harvey, G.R. & Ortner, P.B. 1989. Marine humic and fulvic acids: Their effects on remote sensing of ocean chlorophyll. *Limnol. Oceanogr.* 34: 68–81.

Chen, Z., Hu, C. & Muller-Karger, F. 2007. Monitoring turbidity in Tampa Bay using MODIS/Aqua 250-m imagery. *Remote Sens. Environ.* 109: 207–220.

Cole, J., Prairie, Y., Caraco, N., McDowell, W., Tranvik, L., Striegl, R., Duarte, C., Kortelainen, P., Downing, J., Middelburg, J. & Melack, J. 2007. Plumbing the global carbon cycle: Integrating inland waters into the terrestrial carbon budget. *Ecosystems* 10: 171–184.

Cox, R.M., Forsythe, R.D., Vaughan, G.E. & Olmsted, L.L. 1998. Assessingwater quality in Catawba River reservoirs using Landsat thematic mapper satellite data. *Lake Reserv. Manage.* 14: 405–416.

Dall'Olmo, G. & Gitelson, A.A. 2005. Effect of bio-optical parameter variability on the remote estimation of chlorophyll-a concentration in turbid productive waters: experimental results. *Appl. Optics* 44: 412–422.

Dall'Olmo, G. & Gitelson, A. A. 2006a. Effect of bio-optical parameter variability and uncertainties in reflectance measurements on the remote estimation of chlorophyll-*a* concentration in turbid productive waters: modeling results. *Appl. Optics* 45: 3577–3592.

Dall'Olmo, G. & Gitelson, A.A. 2006b. Absorption properties of dissolved and particulate matter in turbid productive inland lakes, *Proceedings of the Ocean Optics XVIII conference,* Montreal, Quebec, 9-13 October, 2006, 15 p.

Dall'Olmo, G., Gitelson, A. A. & Rundquist D. C. 2003.Towards a unified approach for remote estimation of chlorophyll-a in both terrestrial vegetation and turbid productive waters. *Geophys. Res. Lett.* 30: 1938.

Davies-Colley, R.J. 1988. Measuring water clarity with a black disk. *Limnol. Oceanogr.* 33: 616–623.

Dekker, A. G. 1993. Detection of optical water quality parameters for eutrophic waters by high resolution remote sensing. PhD Thesis. Vrije Universiteit. Amsterdam, The Netherlands. 240 p.

Dekker, A.G. Malthus, T.J., Wijnen, M.M. & Seyhan, E. 1992. Remote sensing as a tool for assessing water quality in Loosdrecht lakes. *Hydrobiologia* 233: 137–159.

Dekker A.G, Vos R.J. & Peters S.W.M. 2002. Analytical algorithms for lake water TSM estimation for retrospective analysis of TM and SPOT sensor data. *Int. J. Remote Sens.* 23: 15–36.

Del Castillo, C.E. & Miller, R. L. 2008. On the use of ocean color remote sensing to measure the transport of dissolved organic carbon by the Mississippi River Plume. *Remote Sens. Environ.* 112: 836–844.

Doerffer, R. 2008. *Analysis of the signal/noise and the water leaving radiance Finnish lakes.* Technical note for the Development of MERIS Lake Water Algorithms-project. 4 p. http://www.brockmann-consult.de/beam-wiki/display/LAKES/Home.

Doerffer, R. & Schiller, H. 2007. The MERIS Case 2 algorithm. *Int. J. Remote Sens.* 28: 517–535.

Doerffer, R., & Schiller, H. 2008a. *MERIS Regional Coastal and Lake Case 2 Water Project Atmospheric correction ATBD* (Algorithm Theoretical Basis Document) 1.0. 41 p. http://www.brockmann-consult.de/beam-wiki/download/attachments/1900548/meris_c2r_atbd_atmo_20080609_2.pdf

Doerffer R. & H. Schiller 2008b. *MERIS Lake Water Project - Lake Water Algorithm for BEAM*, ATBD (Algorithm Theoretical Basis Document) 1.0, 17 p. http://www.brockmann-consult.de/beam-wiki/download/attachments/1900548/ATBD_lake_water_RD20080610.pdf

Downing, J.A., Prairie, Y.T., Cole, J.J., Duarte, C.M., Tranvik, L.J., Striegl, R.G., McDowell, W.H., Kortelainen, P., Caraco, N.F., Melack, J.M. & Middelburg J. 2006. The global abundance and distribution of lakes, ponds, and impoundments. *Limnol. Oceanogr.* 51: 2388–2397.

EN 872. *Water Analysis – Determination of suspended solids*. European Committee for Standardization, Strasbourg, 1996.

EN 27027. *Water quality. Determination of turbidity.* European Committee for Standardization, Strasbourg, 1994.

Effler, S. W., Gelda, R. K., Bloomfield, J. A., Quinn, S. & Johnson, D. L. 2001. Modeling the effects of tripton on water clarity: Lake Champlain. *J. Water Res. Planning* 127: 224–234.

European Union 2000. *The EU Water Framework Directive. Directive 2000/60/EC.* http://ec.europa.eu/environment/water/water-framework/index_en.html.

Ferrari, G.M. & Tassan, S. 1999. A method using chemical oxidation to remove light absorption byphytoplankton pigments. *J. Phycol.* 5: 1090–1098.

Fisher, S. G. 1994. Pattern, process and scale in freshwater ecosystems: some unifying thoughts. In Giller, P. S., Hildrew, A. G. & Raffaelli, D. G. (eds). *Aquatic Ecology—Scale, Pattern and Process.* Blackwell Sciences Ltd, London. pp. 575–592.

Gallie, E. A., & Murtha, P. A., 1992, Specific absorption and backscattering spectra for suspended minerals and chlorophyll-a in Chilko Lake, British Columbia. *Remote Sens. Environ.* 39: 103–118.

Gallegos, C.L., Davies-Colley, R.J. & Gall, M. 2008. Optical closure in lakes with contrasting extremes of reflectance. *Limnol. Oceanogr.* 53: 2021–2034.

Gege, P. 1998. Characterization of the phytoplankton in Lake Constance for classification by remote sensing. *Archiv für Hydrobiologie - Advances in Limnology* 53: 179–193.

Gege, P. 2000. Gaussian model for yellow substance absorption spectra. *Proceedings of the Ocean Optics XV Conference*, October 16-20, Monaco. CD-ROM. 9 p.

Gege, P. 2002. Error propagation at inversion of irradiance reflectance spectra in Case-2-waters, *Proceedings of the Ocean Optics XVI Conference*, Santa Fe, New Mexico, November 18-22, 2002. 10 p. [CD-ROM].

GEO 2007. *GEO Inland and Nearshore Coastal Water Quality Remote Sensing Workshop*. 27-29 March 2007, Geneva, Switzerland. Final Report. Group on Earth Observations. 30 p. http://www.earthobservations.org/meetings/20070327_29_water_quality_workshop_report.pdf

GEO 2011. *Progress Report on GEO Inland and Near-Coastal Water Quality Remote Sensing Working Group*. Group on Earth Observations. 13 p. http://www.earthobservations.org/documents/sbas/wa/201101_coastal_and_inland_wq_remote_sensing_wg_progress_report.pdf

Giardino, C., Brando, V.E., Dekker, A.G., Strömbeck, N. & Candiania, G. 2007. Assessment of water quality in Lake Garda (Italy) using Hyperion. *Remote Sens. Environ.* 109: 183–195.

Gitelson A. 1992. The peak near 700 nm on radiance spectra of algae and water: relationships of its magnitude and position with chlorophyll concentration. *Int. J. Remote Sens.* 13: 3367–3373.

Gitelson, A., Dall'Olmo, A. G., Moses, W., Rundquist, D.C., Barrow, T.,Fisher, T.R., Gurlin D. & Holz, J. 2008. A simple semi-analytical model for remote estimation of chlorophyll-a in turbid waters: Validation. *Remote Sens. Environ.* 112: 3582–3593.

Gitelson, A., Szilagyi, F. & Mittenzway, K. 1993. Improving Quantitative Remote Sensing for Monitoring of Inland Water Quality. *Water Res.* 7: 1185–1194.

Gons, H.J, Rijkeboer, M. & Ruddick, K. 2002. A chlorophyll-retrieval algorithm for satellite imagery (Medium Resolution Imaging Spectrometer) of inland and coastal waters. *J. Plankton Res.* 24: 947–951.

Gordon, H.R., Brown, O.B. & Jacobs, M.M. 1975. Computed relationships between the inherent and apparent optical properties of a flat, homogenous ocean. *Appl. Optics* 14: 417–427.

Gordon, H. R. & Ding, K. 1992. Self-shading of in-water optical instruments. *Limnol. Oceanogr.* 37: 491–500.

Gordon, H. R. & Morel, A. 1983. *Remote assessment of ocean color for interpretation of satellite visible imagery: A review*. Lecture notes on coastal and estuarine studies, vol. 4, Springer Verlag, New York. 114 p.

Grassl, H., Pozdnyakov, D., Lyaskovsky, A. & Pettersson, L. 2002. Numerical modelling of transspectral processes in natural waters: Implications for remote sensing. *Int. J. Remote Sens.* 23: 1581–1607.

Green, S.A. & Blough, N.V. 1994. Optical absorption and fluorescence of chromophoric dissolved organic matter in natural waters. *Limnol. Oceanogr.* 39: 1903–1916.

Griffin, C. G., Frey, K. E., Rogan, J. & Holmes, R. M. 2011. Spatial and interannual variability of dissolved organic matter in the Kolyma River, East Siberia, observed using satellite imagery. *J. Geophys. Res.*116: G03018. 12 p.

Guanter, L., Ruiz-Verdú, A., Odermatt, D., Giardino, C., Simis, S., Estellés, V., Heege, T., Domínguez-Gómez, J.A. & Moreno, J. 2010. Atmospheric correction of ENVISAT/MERIS data over inland waters: Validation for European lakes. *Remote Sens. Environ.* 114: 467–480.

de Haan, J.F., & Kokke, J.M. 1996. *Remote Sensing Algorithm Development Toolkit I, Operationalization of Atmospheric Correction Methods for Tidal and Inland Waters*, BCRS Report, RWS-Survey Department, Netherlands. 91 p.

Hansell, D.A. & Carlson, C.A. 2002. *Biochemistry of Marine Dissolved Organic Matter.* Elsevier Science, Academic Press. San Diego. 774 p.

Heege, T. & Fischer, J. 2004. Mapping of water constituents in Lake Constance using multispectral airborne scanner data and a physically based processing scheme. *Can. J. Remote Sens.* 30: 77–86.

Herlevi, A. 2002. *Inherent and apparent optical properties in relation to water quality in nordic waters*. Academic Dissertation, December 2002. Department of Geophysics, University of Helsinki. 57 p.

Hirtle, H. & Rencz, A. 2003. The relation between spectral reflectance and dissolved organic carbon in lake water: Kejimkujik National Park, Nova Scotia, Canada. *Int. J. Remote Sens.* 24: 953–967.

Hoge, F.E. & Lyon, P.E. 1996. Satellite retrieval of inherent optical properties by linear matrix inversion of oceanic radiance models: An analysis of model and radiance measurement errors. *J. Geophys. Res.* 101: 16631–16648.

Holmes, R.W. 1970. The Secchi disk in turbid coastal waters. *Limnol. Oceanogr.* 15: 688–694.

Højerslev, N. K. 1986. Visibility of the sea with special reference to the Secchi Disc. *Proceedings of the Ocean Optics Conference VIII*, Orlando, USA. SPIE Vol. 637, pp. 294–305.

Hoogenboom, H.J., Dekker, A.G., & Althuis, I.J.A. 1998a. Simulation of AVIRIS sensitivity for detecting chlorophyll over coastal and inland waters. *Remote Sens. Environ.* 65: 333–340.

Hoogenboom, H. J., Dekker, A. G. & De Haan, J F. 1998b. Retrieval of chlorophyll a and suspended matter in inland waters from CASI data by matrix inversion. *Can. J. Remote sensing* 24: 144–152.

Härmä, P., Vepsäläinen, J., Hannonen, T., Pyhälahti, T., Kämäri, J., Kallio, K., Eloheimo, K. & Koponen, S. 2001. Detection of water quality using simulated satellite data and semi-empirical algorithms in Finland. *Science Total Environ.* 268: 107–121.

IPPC 2001. The carbon cycle and atmospheric carbon dioxide. In: *Intergovernmental Panel on Climate Change (IPCC), Climate Change 2001*. Cambridge university press, Cambridge. pp. 183–237.

ISO 7887. *Water quality. Examination and determination of colour.* International Standards Organization, Geneva, 1994.

ISO 10260. *Water quality – Measurement of biochemical parameters – Spectrometric determination of the chlorophyll a concentration.* International Organization for Standardization, Geneva, 1992.

Jaun, L., Finger, D., Zeh, M., Schurter, M. & Wuest, A. 2007. Effects of upstream hydropower operation and oligotrophication on the light regime of a turbid peri-alpine lake. *Aquat. Sci.* 69: 212–226.

Jerlov, N. 1976. *Marine optics.* Amsterdam. Elsevier. 231 p.

Jupp, D., Kirk, J.T.O. & Harris, G.P., 1994. Detection, identification and mapping cyanobacteria - using remote sensing to measure the optical quality of turbid inland waters. *Australian Journal Mar. Freshwater Res.* 45: 801–828.

Kallio, K. 1999. Absorption properties of dissolved organic matter in Finnish lakes. *Proceedings of Estonian Academy of Science. Ecology* 48: 75–83.

Kallio, K., Koponen, S., Ruiz-Verdú, A., Heege, T., Sørensen, K., Pyhälahti, T. & Doerffer, R. 2007. *Validation protocol for the Development of MERIS lake water algorithms-project.* European Space Agency. 13 p. http://www.brockmann-consult.de/beam-wiki/display/LAKES/Validation+report

Kallio, K., Koskiaho, J., Lepistö, A., Kiirikki, M. & Tattari, S. 2010. Mitä uutta nykytekniikalla saadaan selville valuma-alue-järvi kokonaisuudesta. In: Lepistö, A., Huttula, T., Granlund, K., Kallio, K., Kiirikki, M., Kirkkala, T., Koponen, S., Koskiaho, J., Liukko, N., Malve, O., Pyhälahti, T., Rasmus, K. & Tattari, T. New environmental research and monitoring methods – a pilot study in the Säkylän Pyhäjärvi area. *Suomen ympäristö* 9/2010, Finnish Environment Institute. pp. 10-18. (In Finnish with English abstract). http://www.ymparisto.fi/download.asp?contentid=117542&lan=fi

Kallio, K., Ylöstalo, P., Koponen, S. & Pyhälahti, T. 2009. Additional test of the MERIS Boreal Lake Processor using Finnish validation data. *Proceedins of the Remote Sensing of the Baltic Sea Workshop,* Tallinn, 20-21.8.2009. 1 p.

Kirk J. 1984. Dependence of relationship between inherent and apparent optical properties of water on solar altitude. *Limnol. Oceanogr.* 29: 350-356.

Kirk, J. 1994. *Light and photosynthesis in aquatic ecosystems.* Cambridge University Press, Second edition. 509 p.

Kloiber, S.M., Brezonik, P.L., Olmanson, L.G. & Bauer, M.E. 2002a. A procedure for regional lake water clarity assessment using Landsat multispectral data. *Remote Sens. Environ.* 82: 38–47.

Kloiber, S. M., Brezonik, P. L. & Bauer, M. E. 2002b. Application of Landsat imagery to regional-scale assessment of lake clarity. *Water Res.* 36: 4330–40.

Koponen, S., Attila, J., Pulliainen, J., Kallio, K. Pyhälahti, T., Lindfors, A., Rasmus, K. & Hallikainen, J. 2007. A case study of airborne and satellite remote sensing of a spring bloom event in the Gulf of Finland. *Cont. Shelf Res.* 27: 228–244.

Koponen, S., Kallio, K., Pulliainen, J., Vepsäläinen, J., Pyhälahti, T. & Hallikainen, M. 2004. Water quality classification of lakes using 250-m MODIS data. *IEEE Geosc. Remote Sens. Lett.* 1: 287–291.

Koponen, S., Ruiz-Verdu, A., Heege, T., Heblinski, J., Sørensen, K., Kallio, K., Pyhälahti, T., Doerffer, D., Brockmann, C. & Peters, M. 2008. *Development of MERIS Lake Water Algorithms. Validation Report.* ESA ESRIN Contract No. 20436/06/I-LG. 65 p. http://www.brockmann-consult.de/beam-wiki/display/LAKES/Validation+report.

Korosov, A., Pozdnyakov, D., Pettersson, L., & Grassl, H. 2007. Satellite-data-based study of seasonal and spatial variations of water temperature and water quality parameters in Lake Ladoga. *J. Appl. Remote Sens.* 1, article number 011508.

Kutser, T. 1997. Estimation of water quality in turbid inland and coastal waters by passive optical remote sensing. PhD Thesis. *Dissertationes Geophysicales Universitatis Tartuensis* 8. University of Tartu, Estonia. 69 p

Laanen, M.L. 2007. *Yellow Matters - Improving the remote sensing of Coloured Dissolved Organic Matter in inland freshwaters.* PhD Thesis. Vrije Universiteit, Amsterdam. 256 p. http://dare.ubvu.vu.nl/handle/1871/10799.

Lepistö, A., Huttula, T., Koponen, S., Kallio, K., Lindfors, A., Tarvainen, M. & Sarvala, J. 2010. Monitoring of spatial water quality in lakes by remote sensing and transect measurements. *Aquat. Ecosyst. Health* 13: 176–184.

Lindfors, A., Rasmus, K. & Strömbeck, N. 2005. Point or pointless: quality of ground data. *Int. J. Remote Sens.* 26: 415–423.

Loisel, H. & Morel A. 2001. Non-isotropy of the upward-radiance field in typical coastal case 2 waters. *Int. J. Remote Sens.* 22: 275–295.

Luyten, P. J., Jones, J. E., Proctor, R., Tabor, A., Tett, P. & Wild-Allen, K. 1999. *COHERENS - A coupled hydrodynamical-ecological model for regional and shelf seas: User documentation.* Report of the Management Unit of the Mathematical Models of the North Sea (MUMM). 911 p.

Maffione, R.A. & Jaffe, J.S. 1995. The average cosine due to an isotropic light source in the ocean. *J. Geophys. Res.* 100: 13179–13192.

Metsamaa, L., Kutser, T. & Strömbeck, N. 2006. Recognising cyanobacterial blooms based on their optical signature: a modelling study. *Boreal Environ. Res.* 11: 493–506.

Millie, D.F.., Baker, M.C., Tucker, C.S., Vinyard, B.T. & Dionogi, C.P. 1992. High-resolution airborne remote sensing of bloom-forming phytoplankton. *J. Phycol.* 28: 281–290.

Milton, J.S. & Arnold, J.C. 1995. *Introduction to probability and statistics: Principles and applications for engineering and computer sciences.* McGraw-Hill Publishing Company, Singapore. 811 p.

Ministry of the Environment 2011. Monitoring strategy of the state of the environment 2020. *Reports of Ministry of the Environment 23/2011*. 75 p. (In Finnish with English summary). http://www.ymparisto.fi/download.asp?contentid=128477&lan=fi.

Mobley, C. D. 1994. *Light and water; radiative transfer in natural waters.* Academic Press, San Diego. 592 pp.

Mobley C.D., Stramski, D., Bissett, W.P. & Boss, E. 2004. Optical Modeling of Ocean Waters: Is the Case 1- Case 2 Classification Still Useful? *Oceanography* 17: 60–67.

Mobley, C.D. & Sundman, L.K. 2007. *Hydrolight 4.3 Users' quide.* Sequoia Scientific, Inc. 88 p.

Morel, A. 1988. Optical modeling of the upper ocean in relation to its biogenous matter content (case 1 waters). *J. Geophys. Res.* 93: 749–768.

Morel, A. & Gentili, B. 1996. Diffuse reflectance of oceanic waters. 3. Implication of bidirectionality for the remote-sensing problem. *Appl. Optics* 35: 4850–4862.

Morel, A. & Prieur, L. 1977. Analysis of variation in water colour. *Limnol. Oceanogr.* 22: 709–722.

Moses, W.J., Gitelson, A.A., Berdnikov, S. & Povazhnyy, V. 2009. Satellite Estimation of Chlorophyll-a Concentration Using the Red and NIR Bands of MERIS—The Azov Sea Case Study. *IEEE Geosc. Remote Sens. Lett. 6:* 845–849.

Mäkisara, K., Meinander, M., Rantasuo, M., Okkonen, J., Aikio, M., Sipola, K., Pylkkö, P. & Braam, B. 1993. *Airborne Imaging Spectrometer for Applications (AISA)*, IGARSS Digest, Tokyo, 1993, pp. 479–481.

NASA 2003. *Ocean Optics Protocols For Satellite Ocean Color Sensor Validation*. Revision 4. http://oceancolor.gsfc.nasa.gov/DOCS/.

Nelder, J.A. & Mead, R. 1965. A simplex method for function minimization. *Comput. J.* **7**: 308–313.
Odermatt, D., Giardino, C. & Heege, T. 2010. Chlorophyll retrieval with MERIS Case-2-Regional in perialpine lakes. *Remote Sens. Environ.* 114: 467 – 480.
Oishi, T., Takahashi, Y. Tanaka, A., Kishino, M. & Tsuchiya, A. 2002. Relation between the backward- as well as total scattering coefficients and the volume scattering functions by cultured phytoplankton. *J. School Mar. Sci. Technol. Tokai Univ*. 53: 1–15.
O'Reilly, J. E., Maritorena, S., Mitchell, B. G., Siegel, D. A., Carder, K. L., Garver, S. A., Kahru, M. & McClain, C. 1998. Ocean color chlorophyll algorithms for SeaWiFS. *J. Geophys. Res.* 103(C11): 24937–24954.
Pegau, W. S., Gray, D. & Zaneveld, J. R. V. 1997. Absorption and attenuation of visible and near-infrared light in water: dependence on temperature and salinity. *Appl. Optics* 36: 6035–6046.
Petzold, T.J. 1972. Volume scattering functions for selected ocean waters. *Scripps Institution of Oceanography. Tech. Rep.* 72–28. 79 p.
Pierson, D., Alberotanza, L., Ferro, G., Kutser, T., Profeti, G., Ramasco, C., & Strömbeck, N. 1999. Optical analyses of water. In: Lindell, T., Pierson, D., Premazzi, G. & Zilioli, E. (eds). *Manual for monitoring European lakes using remote sensing techniques*, EUR Report 18665, Office for Official Publications of the European Communities, Luxembourg. pp. 29–80.
Pierson, D.C., Markensten, H. & Strömbeck, N. 2003. Long and short term variations in suspended particulate material: the influence on light available to the phytoplankton community. *Hydrobiologia* 494: 299–304.
Pierson, D.C. & Strömbeck, N. 2000. A modelling approach to evaluate preliminary remote sensing algorithms: Use of water quality data from Swedish Great Lakes. *Geophysica* 36: 177–202
Pierson, D. & Strömbeck, N. 2001. Estimation of radiance reflectance and the concentrations of optically active substances in Lake Mälaren, Sweden, based on direct and inverse solutions of a simple model. *Science Total Environ.* 268: 171–188.
Pozdnyakov, D. V. & Grassl, H. 2003. *Colour of inland and coastal waters - a methodology for its interpretation.* Springer. London. 170 p.
Pozdnyakov, D. V., Kondratyev, K. Ya, Bukata, R.P. & Jerome, J. H. 1998. Numerical modeling of natural colour: implications for remote sensing and limnological studies. *Int. J. Remote Sens.* 19: 1913–1932.
Pozdnyakov, , D.V., Korosov, A.A., Pettersson, L.H. & Johannessen, O.M. 2005. MODIS evidences the river runoff impact on the Kara Sea trophy. *Int. J. Remote Sens.* 26: 3641–3648.
Preisendorfer, R. W. 1976. *Hydrologic optics,* Vol. 1. NTIS PB-259 793/8ST. National Technical Information Service NTIS, Springfield, VA, USA. 208 p.
Preisendorfer, R.W. 1986. Secchi disk science; visual optics of natural waters. *Limnol. Oceanogr.* 31: 906–926.
Pulliainen J., Kallio K., Eloheimo K., Koponen S., Servomaa H., Hannonen T., Tauriainen S. & Hallikainen M. 2001. A semi-operative approach to water quality retrieval from remote sensing data. *Science Total Environ.* 268: 79–93.
Raatikainen M. & Kuusisto E. 1988. The number and surface area of lakes in Finland. *Terra* 102: 97–110. (In Finnish with English abstract).
Rahman, H. & Dedieu G., 1994. SMAC: A Simplified Method for the Atmospheric Correction of Satellite Measurement s in the Solar Spectrum. *Int. J. Remote Sens.* 15: 123–143.
Reinart, A., Paavel, B., Pierson, D. & Strömbeck, N. 2004: Inherent and apparent optical properties of Lake Peipsi, Estonia. *Boreal Env. Res.* 9: 429–445.
Rijkeboer, M., Dekker, A.G. & Gons, H.J. 1998. Subsurface irradiance reflectance spectra of inland waters differing in morphometry and hydrology. *Aquat. Ecol.* 31: 313–323
Roesler, C. S., Perry, M. J. & Carder, K. L., 1989. Modeling *in situ* phytoplankton absorption from total absorption spectra. *Limnol. Oceanogr.* 34: 1512–1525.
Rowan, K.S. 1989. *Photosynthetic pigments of phytoplankton.* Cambridge University Press. Cambridge. 334 p.
Ruddick, G., Gons, H.J., Rijkeboer, M. & Tilstone, G. 2001. Optical remote sensing of chlorophyll *a* in case 2 waters by use of an adaptive two–band algorithm with optimal error properties. *Appl. Optics* 40: 3575–3585.
Röttgers, R. & Doerffer, R. 2007. Measurements of optical absorption by chromophoric dissolved organic matter using a point-source integrating-cavity absorption meter. *Limnol. Oceanogr. Methods* 5: 126–135.
Santer, R. & Schmechtig, C. 2000. Adjacency effects on water surfaces: primary scattering approximation and sensitivity study. *Appl. Optics* 39: 361–375.
Santer, R. & Zagolski, F. 2008. *ICOL Algorithm Theoretical Base Document, Version 1.1.* ULCO Université du Littoral Côte d'Opale, Wimereux, France. 15 p. http://www.brockmann-consult.de/beam-wiki/download/attachments/13828113/ICOL_ATBD_1.1.pdf
Sathyendranath, S., Prieur, L. & Morel A. 1989. A 3 component model of ocean color and its application to remote-sensing of phytoplankton pigments in coastal waters. *Int. J. Remote Sens.* 10**:** 1373–1394.
Sawaya, K.E., Olmanson., L.G., Heinert, N.J., Brezonik. P.L. & Bauer, M.E. 2003. Extending satellite remote sensing to local scales: Land and water resource monitoring using high-resolution imagery. *Remote Sens. Environ.* 88: 144–156.
Schiller, H. & Doerffer, R. 1999. Neural network for emulation of an inverse model operational derivation of Case II water properties from MERIS data. *Int. J. Remote Sens.* 20: 1735–1746.
Shuchman, R.A., Korosov, A., Hatt, C., Pozdnyakov, D., Means, J. & Meadows, G . 2006 . Verification and application of a bio-optical algorithm for Lake Michigan using SeaWiFS: a 7-year inter-annual analysis. *J. Great Lakes Res.* 32: 258–279.
Simis, S. 2006. *Blue-green catastrophe: remote sensing of mass viral lysis of cyanobacteria.* Ph.D. Thesis, Vrije Universiteit Amsterdam. 144 p. http://dare.ubvu.vu.nl/bitstream/1871/10641/1/7574.pdf

Simis, S. G. H., Ruiz-Verdú, A. , Domínguez, J. A., Peña-Martinez, R., Peters, S. W. M. & Gons, H. J. 2007. Influence of Phytoplankton Pigment Composition on Remote Sensing of Cyanobacterial Biomass. *Remote Sens. Environ.* 106: 414–427

Sipelgas, L., Arst, H., Kallio, K., Erm, A., Oja, P. & Soomere, T. 2003. Optical properties of dissolved organic matter in Finnish and Estonian lakes. *Nord. Hydrol.* 34: 361–386.

Stahr, P. A. & Markager, S. 2002. Parameterization of the chlorophyll a-specific in vivo light absorption coefficient covering estuarine, coastal and oceanic waters. *Int. J. Remote Sens.* 25: 5117–5130.

Stedmon, C.A., Markager, S. & Kaas, H. 2000. Optical Properties and Signatures of Chromophoric Dissolved Organic Matter (CDOM) in Danish Coastal Waters. *Estuar. Coast. Shelf S.* 51: 267–278.

Stramski, D., Boss, E., Bogucki, D. & Voss, K.J., 2004. The role of seawater constituents in light backscattering in the ocean. *Prog. in Oceanogr.* 61: 27–56.

Strömbeck, N. 2001. *Water quality and optical properties of Swedish lakes and coastal waters in relation to remote sensing*. PhD. Thesis, Dep. of Limnology, Uppsala University, Uppsala. 27 p.

Strömbeck, N. & Pierson, D. 2001. The effects of variability in the inherent and optical properties on estimations of chlorophyll *a* by remote sensing in Swedish freshwaters. *Science Total Environ.* 268: 123–137.

Tassan, S & Ferrari, G.M. 2002. A sensitivity analysis of the 'Transmittance-Reflectance' method for measuring light absorption by aquatic particles. *J. Plankton Res.* 24: 757–774.

Thiemann, S. & Kaufmann, H. 2000. Determination of chlorophyll content and trophic state of lakes using field spectrometer and IRS-1C satellite data in the Mecklenburg Lake District, Germany. *Remote Sens. Environ.* 73: 227–235.

Tilak, S., Arzberger, P., Balsiger, D., Benson, B., Bhalerao, R., Chiu, K., Fountain, T., Hamilton, D., Hanson, P., Kratz, T., Lin, F.P., Meinke, T. & Winslow, L. 2007. Conceptual Challenges and Practical Issues in Building The Global Lake Ecological Observatory Network. *Proceedings of the Third International Conference on Intelligent Sensors, Sensor Networks and Information Processing* (ISSNIP), Melbourne, Australia. 6 p. http://www.gleon.org/media/gleon-issnip07.pdf

Twardowski, M.S., Boss, E., Sullivan, J.M. & Donaghay, P.L. 2004. Modeling the spectral shape of absorption by chromophoric dissolved organic matter. *Mar. Chem.* 89: 69–88.

Twardowski, M. S. & Donaghay, P. L. 2002. Photobleaching of aquatic dissolved materials: Absorption removal, spectral alteration and their interrelationship. *J. Geophys. Res.* 107(C8): 3091.

Tyler, J.E. 1968. The Secchi disk. *Limnol. Oceanogr.* 13: 1–6.

Vaillancourt, R.D., Brown, C.W., Guillard, R.R.L. and Balch, W.M. 2004 Light backscattering properties of marine phytoplankton: relationships to cell size, chemical composition and taxonomy. *J. Plankton Res.* 26: 191–212.

Van Der Woerd, H. J. & Pasterkamp, R. 2008. HYDROPT: A fast and flexible method to retrieve chlorophyll-a from multispectral satellite observations of optically complex coastal waters. *Remote Sens. Environ.* 112: 1795–1807.

Van Stokkom, H. T. C., Stokman, G. N. M. & Hovenier, J. W. 1993, Quantitative use of passive optical remote sensing over coastal and inland water bodies. *Int. J. Remote Sens.* 14: 541–563.

Vincent, R.K., Qin X., McKay, R.M.L., Miner, J., Czajkowski, K., Savino, J. & Bridgeman, T. 2004. Phycocyanin detection from Landsat TM data for mapping cyanobacterial blooms in Lake Erie. *Remote Sens. Environ.* 89: 381–392.

Vuori K.-M. 2009. Pintavesiemme tila uusien luokitteluperusteiden valossa (The status of our surface water in the light of new classification criteria). *Vesitalous* 2/2009: 11–15. In Finnish.

Vuoristo, H. 1998. Water quality classification of Finnish inland waters. *European Water Management* 1: 35–41.

Vähätalo A. V., Salkinoja-Salonen, M., Taalas, P. & Salonen, K.. 2000. Spectrum of the quantum yield for photochemical mineralization of dissolved organic carbon in a humic lake. *Limnol. Oceanogr.* 45: 664–676.

WET Labs 1995. *ac-9 user's manual*, Version 1.0. Philomath, Oregon, USA. 41 p.

Whitmire, A. L, Boss, E., Cowles, T. J. & Pegau, W. S. 2007. Spectral variability of the particulate backscattering ratio. *Optics Express* 15: 7019–7031.

Ylöstalo, P., Kallio, K. & Seppälä, J. 2011. *Absorption properties of particles and CDOM in Finnish lakes.* Manuscript.

Zhang, Y. Longqing F., Junsheng L., Liancong L., Yan Y., Mingliang L. & Yunliang L. 2010. Seasonal–spatial variation and remote sensing of phytoplankton absorption in Lake Taihu, a large eutrophic and shallow lake in China. *J. Plankton Res.* 32: 1023–1037.

Appendix

Appendix. The concentrations of CPSs, Z_{SD}, K_d(PAR) and b_{tot}(555) of the optical stations (**PI**) (b_{tot}(555) was measured by ac-9 and is presented without pure water).

Lake	Station	Month	C_{TSS} mg l^{-1}	$C_{Chl\text{-}a}$ ug l^{-1}	$a_{cdom}(400)$ m^{-1}	Z_{SD} m	$K_d(PAR)$ m^{-1}	$b_{tot}(555)$ m^{-1}
Puujärvi	Puu-m*	May	1.9	4.5	2.1	3.9	1.1	1.2
Lohjanjärvi	Loh1-a*	August	15.5	55	5.3	0.8	3.8	6.6
Lohjanjärvi	Loh2-a*	August	4.6	13.5	3.8	1.5	1.9	2.6
Lohjanjärvi	Loh3-a*	August	5.9	10.5	3.9	1.9	2.0	2.5
Lohjanjärvi	Loh4-a*	August	3.0	11.5	3.3	2.9	1.0	1.9
Enäjärvi	Ena-a*	August	10	37	1.9	1.1	2.8	7.9
Norvajärvi	Nor1-a*	August	0.8	3.5	3.1	4.0	1.5	1.0
Norvajärvi	Nor2-a*	August	1.1	3.3	3.6	3.3	1.5	0.9
Sierijärvi	Sie-a*	August	19.6	73	18.2	0.4	7.8	-
Sonkajärvi	Son-a*	August	1.7	5.7	13.0	2.2	3.9	1.7
Pöyliöjärvi	Poy-a*	August	1.0	7.6	10.0	2.5	3.0	1.2
Vasikkajärvi	Vas-a*	August	0.4	0.8	0.3	11.8	0.6	0.3
Lohjanjärvi	Loh1-m	May	17	9.7	9.2	0.8	-	8.1
Lohjanjärvi	Loh2-m	May	10	7.2	5.4	1.1	-	4.5
Lohjanjärvi	Loh3-m	May	7.8	4.2	4.8	1.2	-	3.6
Keravanjärvi	Ker-m	May	4.4	8.8	14.3	1.4	-	2.8
Puujärvi	Puu-a	August	1.7	1.3	1.3	7.0	0.8	0.9
Vesijärvi	Ves-a	August	2	11.5	1.4	2.8	-	2.1
Pääjärvi	Paa1-a	August	2.1	5.5	7.4	2.7	-	1.4
Pääjärvi	Paa2-a	August	1.6	6.8	7.2	2.7	2.7	1.4

* Stations used for testing of the reflectance model.

ISBN 978-952-11-3947-5 (print.)
ISBN 978-952-11-3948-2 (PDF)
ISSN 1239-1875 (print.)
ISSN 1796-1661 (online)

MONOGRAPHS of the Boreal Environment Research No. 39 2012